Distinct cellular expression and subcellular localization of Kv2 voltage-gated K^+ channel subtypes in dorsal root ganglion neurons conserved between mice and humans

Robert G. Stewart[1], Miriam Camacena[1], Bryan A. Copits[2], Jon T. Sack[1,3]

Affiliations:

[1] Department of Physiology and Membrane Biology, University of California Davis, Davis, CA 95616, USA.

[2] Washington University Pain Center, Washington University School of Medicine, St. Louis, MO 63110, USA; Department of Anesthesiology, Washington University School of Medicine, St. Louis, MO 63110, USA.

[3] Department of Anesthesiology and Pain Medicine, University of California Davis, Davis, CA 95616, USA.

Corresponding author email: jsack@ucdavis.edu

Pages in manuscript: 82

Number of figures: 11

Number of supplemental figures: 12

Number of tables: 2

Number of words in abstract: 248

Number of words in introduction: 601

Number of words in discussion: 1119

Conflict of interest statement: The authors declare no competing conflicts of interest.

Acknowledgments:

We thank James S. Trimmer (University of California, Davis) for generous provision of antibodies, numerous discussions, and feedback on the manuscript. We thank Michael Ferns (University of California, Davis) for feedback on the manuscript. We thank the human tissue donor and their family for their generous donations to science. We thank Jiwon Yi, Zack Bertels, Maria Payne, and Jon Lemen for performing hDRG extractions. GxTX was synthesized at the Molecular Foundry of the U.S. Department of Energy under contract DE-AC02-05CH11231. This research was supported by U.S. National Institutes of Health grant R01NS096317 to J.T. Sack and the University of California, Davis.

Author contributions: R. G. Stewart: Conceptualization, formal analysis, investigation, methodology, visualization, writing-original draft, writing-reviewing and editing. M. Camacena: investigation. B. A. Copits investigation, writing-reviewing and editing. J.T. Sack: Conceptualization, formal analysis, funding acquisition, investigation, methodology, project administration, supervision, visualization, writing-original draft, writing-reviewing and editing.

ABSTRACT

The distinct organization of Kv2 voltage-gated potassium channels on and near the cell body of brain neurons enables their regulation of action potentials and specialized membrane contact sites. Somatosensory neurons have a pseudo unipolar morphology that allows transmitted action potentials to bypass the cell body. Kv2 channels regulate action potentials in somatosensory neurons, yet little is known about where Kv2 channels are located. Here we define the cellular and subcellular localization of the Kv2 paralogs, Kv2.1 and Kv2.2, in dorsal root ganglia (DRG) somatosensory neurons with a panel of antibodies, cell markers, and genetically modified mice. We find that relative to spinal cord neurons, DRG neurons have similar levels of detectable Kv2.1, and higher levels of Kv2.2. In older mice, detectable Kv2.2 remains similar while detectable Kv2.1 decreases. Both Kv2 subtypes adopt clustered subcellular patterns that are distinct from central neurons. Kv2.2 is distinct in being found at juxtaparanodes and paranodes of myelinated axons. Most DRG neurons co-express Kv2.1 and Kv2.2, although neuron subpopulations show preferential expression of Kv2.1 or Kv2.2. We find that Kv2 protein expression and subcellular localization is similar between mouse and human DRG neurons. We conclude that the organization of both Kv2 channels is consistent with physiological roles in the somata and stem axons of DRG neurons. The general prevalence of Kv2.2 in DRG as compared to central neurons and the enrichment of Kv2.2 relative to detectable Kv2.1, in older mice, proprioceptors, and myelinated axons suggest more widespread roles for Kv2.2 in DRG neurons.

56 **Significance statement**

57

58 The subcellular distribution of Kv2 voltage-gated potassium channels enable compartment-
59 specific modulation of membrane excitability and organization of membrane contact sites. Here
60 we identify subcellular distributions of the Kv2 paralogs, Kv2.1 and Kv2.2, in somatosensory
61 neurons that bear similarities to and distinctions from central neurons. The distribution of Kv2
62 channels is similar in mouse and human somatosensory neurons. These results identify unique
63 locations of Kv2 channels in somatosensory neurons that could enable roles in sensory
64 information processing.

65 **INTRODUCTION**

66

67 The subcellular localization of voltage-gated ion channels in neurons determines how electrical signals
68 are propagated. The two members of the Kv2 family of voltage gated potassium channels, Kv2.1 and
69 Kv2.2, are important for modulating electrical signals in mammalian somatosensory neurons (Bocksteins
70 et al., 2009; Lee et al., 2020; Sun et al., 2022; Tsantoulas et al., 2014; Zheng et al., 2019), yet little is
71 known about where Kv2 channels are localized in these neurons. In central neurons, Kv2 channels are
72 sequestered to specific subcellular regions and identification of where these channels are has helped
73 elucidate their functional roles (Bishop et al., 2015; Du, Tao-Cheng, Zerfas, & McBain, 1998; Irie, 2021;
74 Jensen et al., 2017; Johnson et al., 2018; Kihira, Hermanstyne, & Misonou, 2010; Kirmiz, Vierra, Palacio,
75 & Trimmer, 2018; Misonou, Mohapatra, Menegola, & Trimmer, 2005; Muennich & Fyffe, 2004; Romer et
76 al., 2014; Scannevin, Murakoshi, Rhodes, & Trimmer, 1996; Trimmer, 1991; Vierra, O'Dwyer,
77 Matsumoto, Santana, & Trimmer, 2021). Establishing where Kv2 channels are in somatosensory neurons
78 likewise identifies sites where they could function.

79

80 Among vertebrates, the Kv2 family contains two conserved paralogs, Kv2.1 and Kv2.2, which can
81 assemble into homo- or hetero-tetramers to form voltage gated K^+ channels (Blaine & Ribera, 1998;
82 Kihira et al., 2010). In central neurons, Kv2.1 and Kv2.2 channels have unique cellular expression,
83 subcellular localization and show distinct physiological roles (Bishop et al., 2015; Newkirk et al., 2022).
84 Among cortical neuron types, Kv2.1 is more broadly distributed than Kv2.2 (Bishop et al., 2015). Little is
85 known of how Kv2.1 or Kv2.2 channels are distributed among somatosensory neuron subtypes. In
86 central neurons, Kv2.1 and Kv2.2 channels localize in clusters on the cell soma, proximal dendrites, and
87 axon initial segment (Bishop et al., 2015; King, Manning, & Trimmer, 2014; Sarmiere, Weigle, & Tamkun,
88 2008; Scannevin et al., 1996; Trimmer, 1991). Clustered Kv2 channels form endoplasmic reticulum-

89 plasma membrane junctions (Johnson et al., 2018; Kirmiz et al., 2018), where they perform
90 nonconducting functions which include mediating coupling of L-type calcium channels to ryanodine
91 receptors (Vierra et al., 2021), and Ca^{2+} uptake (Panzera et al., 2022). In somatosensory neurons it
92 remains unknown whether Kv2 channels form organized structures or are localized to specific
93 subcellular compartments. Identifying if channel expression is specific to neuron subtypes and within
94 specific subcellular domains could indicate whether Kv2.1 and Kv2.2 channels also have distinct
95 physiological roles in somatosensory neurons.
96
97 Kv2 channels are expressed and play important functional roles in DRG. Kv2 transcripts have been
98 detected in all classes of DRG neurons with a notable absence of Kv2.1 mRNA in proprioceptors (Usoskin
99 et al., 2015; Wangzhou et al., 2020; Zheng et al., 2019). Presence of Kv2.1 protein in DRG of mice and
100 rats has been identified by western blot and immunohistochemistry respectively (Sun et al., 2022;
101 Tsantoulas et al., 2012). Pharmacological inhibition of Kv2 channels enhances rat DRG neuron
102 responsiveness to sustained inputs (Tsantoulas et al., 2014). Kv2 conductances have been identified in
103 several mouse DRG neuron subtypes (Bocksteins et al., 2009; Regnier, Bocksteins, Van de Vijver,
104 Snyders, & van Bogaert, 2016; Zheng et al., 2019). Kv2 channels have also been implicated in
105 nociception. Kv2.1 and Kv2.2 mRNA transcript levels are decreased after peripheral axotomy of rat DRG
106 neurons (Tsantoulas et al., 2014). Suppression of Kv2.1 transcription by the epigenetic factor Cdyl is
107 implicated in regulating pain sensation (Sun et al., 2022). A missing piece of the puzzle of how Kv2
108 channels are involved in somatosensory neuron function is the location of the channels themselves.
109 Here we use antibodies against Kv2.1 and Kv2.2 to define their cellular expression and subcellular
110 localization in DRG neurons of both mice and humans.

111 **MATERIALS AND METHODS**

112

113 ***Mice***

114 This study was approved by the UC Davis Institutional Animal Care and Use Committee and conforms to
115 guidelines established by the NIH. Mice were maintained on a 12 h light/dark cycle, and food and water
116 was provided *ad libitum.* Kv2.1 KO and Kv2.2 KO mice were from breeding Kv2.1+/- or Kv2.2+/-
117 heterozygous mice such that WT mice were from breeding pairs that generated KO mice. Kv2.1 and Kv2.2
118 DKO mice were generated from breeding Kv2.1+/- heterozygous and Kv2.2-/- homozygous mice. WT
119 controls for Kv2.1/Kv2.2 DKO experiments were C57BL/6J mice purchased from Jackson Laboratory (stock
120 #000664). The *PV*^{Ai14} mouse line was a generous gift from Dr. Theanne Griffith (University of California
121 Davis, Davis CA) and were a cross of *Rosa26*^{Ai14} (stock #007914, MGI: J:155793) and *PVcre* (stock #008069,
122 MGI:J: 100886) mice. The *MrgprD*^{GFP} mouse line was a generous gift from Dr. David Ginty (Harvard
123 University, Boston MA) (MGI: 3521853). Detailed information about the genotype, age, sex and level of
124 spinal column of mice used in each figure can be found in Table 1.

125

126 ***Human Tissue Collection***

127 Human DRG (L3 spinal level) were obtained in collaboration with Mid-America Transplant (St. Louis, MO)
128 from a 59-year-old black male (cause of death: hemorrhagic stroke). DRG were extracted less than 2
129 hours after aortic cross clamp and transported to the lab where they were dissected to remove the
130 dura, embedded in Optimal Cutting Temperature (OCT) compound, snap frozen, and stored at -80 °C
131 until use (Valtcheva et al., 2016). Human DRG were obtained from organ donors with full legal consent
132 for use of tissue for research in compliance with procedures approved by Mid-America Transplant.

133

134 ***Tissue Preparation***

135 Mice were briefly anesthetized with 3-5% isoflurane and then decapitated. The spinal column was
136 dissected, and excess muscle tissue removed. The spinal column was then bisected in the middle of the
137 L1 vertebrae identified by the 13th rib and drop fixed for 1 hour in ice cold PFA: 4% formaldehyde
138 prepared fresh from paraformaldehyde in 0.1 M phosphate buffer (PB) pH adjusted to 7.4 with NaOH.
139 0.1 M PB buffer was diluted from a 0.4 M PB stock solution that was made by diluting 91.37 g of
140 $Na_2H_2PO_4$ and 20.98 g of $Na_2H_2PO_4 \bullet H_2O$ in 2 liters of milliQ water. The relatively short fixation period
141 was chosen because a longer fixation period increased the off target secondary antibody
142 immunofluorescence from mouse isotype secondary antibodies (Figure 1-1). The spine was washed 3×
143 for 10 min each wash in PB and cryoprotected at 4 °C in 30% sucrose in PB for 24 hours. The spine was
144 cut into sections containing two vertebra per sample which were frozen in OCT (Fisher cat#4585) and
145 stored at -80 °C until sectioning. Vertebrae position relative to the 13th rib was recorded for each frozen
146 sample to determine the specific vertebrae position in the spinal cord. Samples were cut into 30 µm
147 sections on a freezing stage sliding microtome and were collected on Colorfrost Plus microscope slides
148 (Fisher cat#12-550-19). Slides were stored at -20 °C or immediately used for multiplex
149 immunofluorescence labeling.

150

151 Human DRG were cut into 30 µm sections on a freezing stage sliding microtome and were collected on
152 Colorfrost Plus microscope slides. Sections were briefly thawed to adhere to the slide but were
153 immediately returned to the cryostat kept at -20 °C. Slides were removed from the cryostat and
154 immediately transferred to freshly made 4% PFA pH 7.4 for 10 minutes. Slides were then placed in PB
155 solution for 10 minutes and immediately used for multiplex immunofluorescence labeling. Attempts at
156 immunolabeling Kv2 channels in human DRG tissue that was fixed in 4% PFA for 24 hours were not
157 successful.

158 ***Neuron Cell Culture***

159 Cervical, thoracic and lumbar DRGs were harvested from mice and transferred to Hank's buffered saline
160 solution (HBSS) (Invitrogen). Ganglia were treated with collagenase (2 mg/ml; Type P, Sigma-Aldrich) in
161 HBSS for 15 min at 37°C followed by 0.05% Trypsin-EDTA (Gibco) for 2.5 min with gentle rotation. Trypsin
162 was neutralized with culture media (MEM, with L-glutamine, Phenol Red, without sodium pyruvate)
163 supplemented with 10% horse serum (heat-inactivated; Gibco), 10 U/ml penicillin, 10 µg/ml streptomycin,
164 MEM vitamin solution (Gibco), and B-27 supplement (Gibco). Serum-containing media was decanted and
165 neurons were triturated using a fire-polished Pasteur pipette in MEM culture media containing the
166 supplements listed above. Neurons were plated on laminin-treated (0.05 mg/ml, Sigma-Aldrich) 35 mm
167 glass bottom dishes (MatTek cat#P35G-1.5-7-C). Neurons were then incubated at 37°C in 5% CO_2. Neurons
168 were used for imaging experiments within 24 hours after plating.

169

170 ***Labeling Endogenous Kv2 in live cultured DRG neurons***

171 Plates were removed from 37°C incubator 24 hours after plating. Neurons were washed once with 1 mL
172 neuronal external (NE) solution (3.5 KCl, 155 NaCl, 10 HEPES, 1.5 CaCl2, and 1 MgCl2, 10 mM glucose
173 adjusted to pH 7.4 with NaOH). Neurons were then incubated with NE solution supplemented with 1%
174 BSA for 5 minutes. Neurons were then washed once with NE solution and incubated in 5 µg/mL wheat
175 germ agglutinin conjugated to Alexa Fluor 405 (Biotium cat#29028-1) diluted in NE solution for 2.5
176 minutes. Neurons were washed twice with NE solution and imaged. NE solution was removed and then
177 neurons were incubated for 10 minutes in 100 nM GxTX-594 prepared as described (Thapa et al., 2021).
178 Neurons were then washed three times in NE solution and imaged again. The temperature of the
179 imaging chamber was 25 °C throughout the experiment. Experimenter was blinded to which culture
180 dishes contained DRG neurons from either WT or Kv2.1/Kv2.2 double knockout mice throughout the
181 experiment and image analysis.

182

183 ***Immunohistochemistry***

184 A hydrophobic barrier was drawn around tissue sections mounted on slides as described above using a
185 hydrophobic barrier pen (Scientific Device cat#9804-02). Sections were incubated in 4% milk, 0.1 M
186 phosphate buffer (PB) and 0.2% Triton X-100 (vehicle) for 1 hour. Sections were then incubated in
187 vehicle containing 0.1 mg/mL IgG F(ab) polyclonal IgG antibody (Abcam cat#ab6668) for 1 hour. We
188 determined that a concentration of 0.1 mg/mL maximally blocked off-target secondary antibody labeling
189 when using isotype-specific anti-mouse secondary antibodies (Figure 1-2). Sections were washed 3× for
190 5 min each in vehicle and then incubated in vehicle containing primary antibodies for 1 hour. Primary
191 antibodies and concentrations used are listed in Table 2. Sections were then washed 3× for 5 min each
192 in vehicle and then incubated in vehicle containing IgG-subclass-specific secondary Abs for one hour
193 (Thermo Fisher). Sections were then washed 3× for 5 min each in PB and mounted with Prolong Gold
194 (Thermo Fisher cat#P36930) and Deckglaser cover glass (Fisher Scientific cat#NC1776158). All
195 incubations and washes were done at room temperature with gentle rocking. Human tissue was
196 immunolabeled identically to mice with the exception that the step incubating sections in vehicle
197 containing 0.1 mg/mL IgG F(ab) polyclonal IgG antibody was omitted and sections were incubated in
198 primary antibodies for 2 hours instead of 1. Primary antibodies used in Figure 2 and Figure 3 were used
199 at saturating concentrations (Figure 2-1).

200 ***Imaging***

201 Images were acquired with an inverted scanning confocal and airy disk imaging system (Zeiss LSM 880
202 Airyscan, 410900-247-075) run by ZEN black v2.1. Laser lines were 405 nm, 488 nm, 543 nm and 633 nm.
203 Low-magnification images to image whole mouse DRG were acquired in confocal or airy disk imaging
204 mode with a 0.8 NA 20x objective (Zeiss 420650-9901) details in figure legends. Images containing both
205 the DRG and spinal cord were tile scan images acquired in confocal mode with the same 20x objective.

206 When imaging whole DRG for Figure 2 and Figure 3 the imaging plane was selected using fluorescence
207 from channels that did not contain anti-Kv2.1 or anti-Kv2.2 immunofluorescence. High-magnification
208 images were acquired in airy disk imaging mode with a 1.4 NA 63x oil objective (Zeiss 420782-9900-799).
209 Linear adjustments to contrast and brightness and average fluorescence intensity z-projections were
210 performed using ImageJ software.

211

212 ***Image Analysis***

213 Images were analyzed using ImageJ software (Schindelin et al., 2012). A summary of automated analysis
214 for selecting neurons in DRG sections can be found in Figure 2-2. The ImageJ plugin MorphoLibJ was
215 used for performing watershed segmentation of images (Legland, Arganda-Carreras, & Andrey, 2016).
216 Unless stated otherwise the region of DRG neurons used to analyze anti-Kv2 immunofluorescence is the
217 outer edge (Figure 2-2 I). Immunofluorescence is defined as the raw pixel values from confocal images
218 and was not background subtracted. We noted that in smaller neurons the nucleus takes up a greater
219 percentage of the total volume and could skew fluorescence measurements if fluorescence in the entire
220 soma volume is measured. As Kv2 protein is not present in the nucleus and is enriched at the outer edge
221 (Figure 1) we found that measuring anti-Kv2 immunofluorescence at the outer edge of the neuron
222 reduces potential error that could be associated with soma diameter. For proteins that were not Kv2
223 channels we analyzed the immunofluorescence of the entire soma as these proteins did not exhibit the
224 same enrichment at the outer edge as Kv2 channels (Figure 10 B). Where specified manual ROIs were
225 used in analysis otherwise automatically generated ROIs were used. When analyzing
226 immunofluorescence from human neurons, ROIs were drawn around areas within the neuronal soma
227 that do not contain apparent lipofuscin (Figure 11-1 C). Fitting of imaging data was performed using Igor
228 Pro software version 8 (Wavemetrics, Lake Oswego, OR) that employs nonlinear least square curve

fitting via the Levenberg-Marquardt algorithm. Distributions of fluorescence intensity from DRG neurons were fit with a log normal distribution:

$$f(x) = A^{-\left[\frac{\ln\left(\frac{x}{x_0}\right)}{width}\right]^2} \qquad \text{(Equation 1)}$$

Where A = amplitude, x_0 = mean, and width = $\sqrt{2}$ times standard deviation. Concentration-effect experiments in Figure 2-1 were fit with the Hill equation:

$$f(x) = base + \frac{max - base}{1 + \left(\frac{x_{half}}{x}\right)^n} \qquad \text{(Equation 2)}$$

Code Accessibility

In house Fiji macros and R script used to process imaging data are available for download at https://github.com/SackLab/DRG-Image-Processing

Statistics

All statistical tests were performed in Igor Pro software version 8 (Wavemetrics, Lake Oswego, OR). Independent replicates (n) are individual neurons while biological replicates (N) are individual mice. The n and N values for each figure are listed in Table 1. Details of statistical tests are in the figure legends.

248 **RESULTS**

249

250 **Kv2.1 and Kv2.2 immunolabeling is enriched at the apparent plasma membrane of DRG neuron**

251 **somata**

252

253 To assess the cellular expression and subcellular localization of Kv2.1 and Kv2.2 voltage gated potassium

254 channels in DRG neurons we used a set of anti-Kv2.1 and anti-Kv2.2 antibodies that have previously

255 been validated in brain tissue from Kv2 knockout mice (Bishop et al., 2015) to perform multiplex

256 immunofluorescence labeling of DRG neurons. Anti-Kv2.1 (magenta) and anti-Kv2.2 (green)

257 immunofluorescence is prominent in DRG neuron somata (Figure 1 A). In most neurons we observed

258 anti-Kv2.1 and anti-Kv2.2 immunofluorescence enriched at the outer edge of DRG neuron somata

259 consistent with their plasma membrane localization (Figure 1 B arrows). This putative cell surface

260 localization is distinct from prior reports of anti-Kv2 immunofluorescence in DRG (Tsantoulas et al.,

261 2012) as well as that for other ion channel proteins such as Nav1.8 (Shields et al., 2012) and TRPV1 (Cho

262 & Valtschanoff, 2008), all of which are primarily in the cytoplasm. Anti-Kv2.1 or anti-Kv2.2

263 immunofluorescence at the edge of neuron somata was more apparent when imaging thinner optical

264 sections. To determine if enrichment of Kv2 immunolabeling at the outer edge of DRG neurons was an

265 artifact of our immunohistochemistry or imaging protocols, we additionally labeled DRG sections with a

266 knockout-validated antibody against Nav1.8. In the same DRG section labeled for Kv2 channels,

267 cytoplasmic anti-Nav1.8 immunofluorescence was prominent in small to medium diameter lumbar DRG

268 neurons, consistent with previous reports (He et al., 2010; Shields et al., 2012) (Figure 1 B). To quantify

269 enrichment of anti-Kv2 versus anti-Nav1.8 immunofluorescence at the outer edge of DRG neurons, we

270 manually drew regions of interest (ROIs) for each DRG soma. We generated a 2 µm wide annulus that

271 encompassed the outer edge and a second 2 µm wide annulus just inside the first one (Figure 1 C arrows

272 1 and 2 respectively). By comparing the fluorescence intensity of immunofluorescence signals within
273 these annuli we found that the edge of DRG neuron somata is enriched for anti-Kv2.1 and anti-Kv2.2
274 immunofluorescence relative to that of Nav1.8 (t-test: Kv2.1:Nav1.8 = $p < 0.001$; Kv2.2:Nav1.8 = $p <$
275 0.001) (Figure 1 D). Similarly, anti-Kv2.1 and anti-Kv2.2 immunofluorescence is enriched at the edge of
276 DRG neuron somata relative to anti-TRPV1 immunofluorescence (t-test: Kv2.1:Nav1.8 = $p < 0.001$;
277 Kv2.2:Nav1.8 = $p < 0.001$) (Figure 1-3).
278
279 **Most dorsal root ganglion neurons express Kv2 protein**
280
281 To determine whether the anti-Kv2.1 immunofluorescence signal in DRG sections is specific and
282 dependent on the presence of Kv2.1 protein, we compared fluorescence intensities in DRG samples
283 prepared in parallel from wild-type (WT) mice and Kv2.1 knock-out (KO) mice. We observed anti-Kv2.1
284 immunolabeling in WT DRG neurons that was absent from Kv2.1 KO, while fluorescence corresponding
285 to an antibody that targets βIII tubulin was similar in both WT and Kv2.1 KO mice (Figure 2 A). To
286 quantify fluorescence intensities of individual neurons, we used an automated method to generate
287 regions of interest (ROIs) at the outer edge of DRG neuron somata. This analysis confirmed a reduction
288 in anti-Kv2.1 but not anti-βIII tubulin immunofluorescence in Kv2.1 KO samples (Figure 2 B and C). In 5
289 mice, anti-Kv2.1 immunofluorescence was significantly reduced in Kv2.1 KO samples relative to WT (t-
290 test $p < 0.0001$) while no significant difference was observed in these samples for anti-Kv2.2 or anti-βIII
291 tubulin immunofluorescence (Figure 2 D).
292
293 We developed a method to estimate the fraction of DRG neurons that express Kv2.1 protein on their
294 outer edge. Fluorescence from Kv2.1 KO neurons labeled with an anti-Kv2.1 antibody had neuron-to-
295 neuron variability which could reasonably be fit with a log normal distribution (equation 1) (Figure 2 E).

296 We assumed a similar distribution of background immunofluorescence is also present in WT DRG
297 neurons and scaled the Kv2.1 KO log normal fit to estimate the fraction of neurons without detectable
298 Kv2.1 (Figure 2 F red gaussian). Using this method we compared Kv2.1 immunofluorescence in DRG
299 sections of age and sex matched WT and Kv2.1 KO mice from the 12th thoracic vertebra and estimated
300 that 84 ± 9% (SD) of DRG neurons have detectable Kv2.1 protein (N = 5 pairs of mice) (Figure 2 G).
301
302 Using the same type of analysis, we found that anti-Kv2.2 immunofluorescence was significantly
303 reduced in Kv2.2 KO mice (Two tailed t-test $p < 0.001$) while no significant difference in anti-NF200 or
304 anti-Kv2.1 immunofluorescence was observed (Figure 3 A-D). Comparing anti-Kv2.2
305 immunofluorescence from WT and Kv2.2 KO mice indicates that 91 ± 5% (SD) of the WT mouse DRG
306 neurons have detectable Kv2.2 protein (N = 8 pairs of mice) (Figure 3 E-G). We did not observe a
307 difference between males and females in detectable Kv2.1 or Kv2.2 protein, but animal numbers were
308 not sufficient for rigorous statistical comparison.
309
310 We validated this methodology with a transgenic MrgprD-GFP mouse line that expresses GFP in non-
311 peptidergic nociceptors that comprise approximately 19-24% of all lumbar DRG neurons (Dirajlal,
312 Pauers, & Stucky, 2003; Dong, Han, Zylka, Simon, & Anderson, 2001; Wang & Zylka, 2009). In comparing
313 the MrgprD-GFP mice to WT C57BL/6J mice we found that 23 ± 15% (SD) of lumbar neurons (N = 4 pairs
314 of mice) had detectable GFP (Figure 2-3).
315
316 **Kv2.1 immunolabelling decreases in older mice while Kv2.2 immunolabelling remains similar**
317
318 Kv2.2 transcript in mouse DRG decreases during postnatal development (Regnier et al., 2016) and Kv2.1
319 protein expression in mouse brain decreases with age (Cotella et al., 2012; Regnier et al., 2016). To

320 identify if Kv2 protein levels in DRG neurons vary between young adult and old mice we compared anti-
321 Kv2.1 and anti-Kv2.2 immunofluorescence from samples subjected to identical immunolabeling and
322 imaging protocols. We observed lower anti-Kv2.1 (Figure 4 A, B and C) in DRG sections from 50 week old
323 mice relative to 7 week old mice. Comparisons with Kv2.1 KO mice indicate that 50 ± 23% (SD) of DRG
324 neurons from 50 week old mice express detectable Kv2.1 protein, significantly less (p = 0.018) than the
325 84 ± 9% (SD) of neurons with detectable Kv2.1 protein from 7-16 week old mice (Figure 4 D). In contrast,
326 similar anti-Kv2.2 immunofluorescence was seen in samples from young adult and old mice (Figure 4 E, F
327 and G). Comparisons with Kv2.2 KO mice indicate that 96 ± 3% of DRG neurons from 50 week old mice
328 express detectable Kv2.2 protein, a weakly significant increase (p = 0.03) from the 88 ± 3% (SD)
329 detectable Kv2.2 protein in DRG neurons from 7-24 week old mice (Figure 4 H).
330
331 **Kv2 channels are expressed on the cell surface of acutely dissociated DRG neurons**
332
333 To determine if Kv2 channels are present on neuron surfaces we labeled live acutely dissociated DRG
334 neurons with a cell-impermeant fluorescent probe which binds Kv2 channels. The probe is a variant of
335 the tarantula peptide guangxitoxin-1E conjugated to Alex Fluor 594 (GxTX-594) which binds to an
336 extracellular site of Kv2.1 and Kv2.2 channels (Thapa et al., 2021). We applied GxTX-594 to live acutely
337 dissociated DRG neurons from WT mice and double knockout (DKO) mice lacking expression of both
338 Kv2.1 and Kv2.2 protein (Figure 5). In WT DRG neurons, we observed fluorescence at the membrane
339 after application of 100 nM GxTX-594 that was not present before the addition of GxTX-594 (Figure 5 A).
340 Wheat germ agglutinin conjugated to Alexa 405 (WGA-405) was used to identify the surface membrane
341 of cultured DRG neurons and confirmed that the GxTX-594 fluorescence observed in WT neurons was
342 cell surface localized (Figure 5 A middle). The cell surface localized fluorescence of GxTX-594 observed in
343 WT neurons was not present in Kv2.1/Kv2.2 DKO neurons (Figure 5 B). To quantify the cell surface-

344 associated fluorescence signals of individual WT and Kv2.1/Kv2.2 DKO neurons, we used an automated
345 method to generate ROIs corresponding to the WGA-405 fluorescence and measured GxTX-594 labeling
346 within this ROI (Figure 5 C). This analysis confirmed a reduction in GxTX-594 fluorescence at the
347 membrane in cultured DRG neurons from Kv2.1/Kv2.2 DKO mice compared to WT mice (Figure 5 D).
348 Similar to the Kv2 immunofluorescence signals from KO mice (Figures 2 and 3), GxTX-594 fluorescence
349 from Kv2.1 /Kv2.2 DKO mice could be reasonably fit with a log normal distribution (equation 1) (Figure 5
350 E). Applying the same method used to estimate the fraction of neurons expressing detectable Kv2.1 and
351 Kv2.2 immunofluorescence we compared cultured DRG neurons of age and sex matched WT and
352 Kv2.1/Kv2.2 DKO mice and estimated that 76 ± 2.4% (SD) of DRG neurons have detectable cell surface
353 GxTX-594 fluorescence (Figure 5 F and G). This indicates that most, if not all, neurons express Kv2
354 channels in their surface membrane, consistent a report of Kv2 conductance in every DRG neuron type
355 assessed (Zheng et al., 2019) .
356
357 **Anti-Kv2.2 immunofluorescence is enriched in DRG neurons relative to spinal cord neurons**
358
359 In mammals, anti-Kv2.1 and anti-Kv2.2 immunofluorescence is apparent in central neurons of the brain
360 (Kihira et al., 2010; Bishop et al., 2015) and anti-Kv2.1 in the spinal cord (Bishop et al., 2015; Muennich &
361 Fyffe, 2004). We measured Kv2 immunofluorescence intensities in sections of mouse spinal column
362 which contain both the DRG and the spinal cord. Neurons in the ventral and dorsal horn of the spinal
363 cord exhibit anti-Kv2.1 immunofluorescence (Figure 6 A). We observed anti-Kv2.1 puncta on neurons in
364 the ventral horn (Figure 6 A inset) similar to that described in alpha motor neurons (Fletcher et al., 2017;
365 Romer et al., 2014). Fewer spinal cord neurons exhibit anti-Kv2.2 immunofluorescence than anti-Kv2.1
366 (Figure 6 A and Figure 6-1 A arrowheads). Kv2.2 channel protein in the spinal cord of mice has to our
367 knowledge not been assessed, but anti-Kv2.2 immunofluorescence has been observed early in

368 development in the ventrolateral spinal cord in the frog *Xenopus laevis* (Gravagna, Knoeckel, Taylor,
369 Hultgren, & Ribera, 2008). We analyzed anti-Kv2 immunofluorescence from individual neurons in the
370 DRG and ventral horn of five mice and found that while anti-Kv2.1 immunofluorescence is similar
371 between the two regions (Figure 6 B), anti-Kv2.2 immunofluorescence is significantly higher in DRG
372 neurons relative to ventral horn neurons (Figure 6 C). Approximately 30% of neurons in the DRG have
373 anti-Kv2.2 immunofluorescence at a level higher than the brightest anti-Kv2.2 immunofluorescence
374 observed in the spinal cord. We repeated this analysis with a different anti-Kv2.2 antibody and found
375 similar results (Figure 6-1).
376
377 **Kv2 channels on DRG neuron somata and stem axons form clustered subcellular patterns with**
378 **similarities to and distinctions from central neurons.**
379
380 In neurons throughout the brain (Trimmer, 1991, Scannevin et al., 1996, Bishop et al., 2015) and motor
381 neurons in the spinal cord (Muennich and Fyffe, 2004), Kv2 channels form punctate structures referred
382 to as clusters. In central neurons, Kv2 clusters localize to the soma, proximal dendrites and axon initial
383 segment (Lim, Antonucci, Scannevin, & Trimmer, 2000; Scannevin et al., 1996; Trimmer, 1991). At
384 clusters, Kv2 channels organize protein signaling complexes and endoplasmic reticulum-plasma
385 membrane junctions (Johnson et al., 2018; Kirmiz et al., 2018; Panzera et al., 2022; Vierra et al., 2021).
386 To determine whether Kv2 channels in DRG neurons form clusters similar to central neurons, we
387 compared *en face* z-projections of Kv2 clusters in DRG neurons and ventral horn neurons in the same
388 spinal cord section (Figure 7). Anti-Kv2.1 immunofluorescence in the ventral horn neurons of these mice
389 resembles previous reports of mice (Fletcher et al., 2017) and rats (Fletcher et al., 2017; Muennich &
390 Fyffe, 2004). In both DRG and spinal cord neurons Kv2.1 and Kv2.2 channels form dense clusters (Figure
391 7 A and B). Kv2 channel clusters in DRG typically appeared smaller than Kv2 clusters in spinal cord.

392 However, we are not certain these observations in fixed tissue represent the in vivo arrangement, as
393 Kv2.1 channels in brain neurons can decluster in the period between sacrifice and fixation (Misonou et
394 al., 2005). In some DRG neurons, we observed donut shaped Kv2.1 and Kv2.2 clusters (Figure 7 B and C
395 insets) which resemble donut shaped Kv2 clusters in interneurons which harbor specialized protein
396 machinery in their center (Vullhorst et al., 2015).
397
398 DRG neurons are distinct from central neurons as they have a single stem axon that exits the cell soma
399 and bifurcates into the central and peripheral axon branches (Ha, 1970). We observed punctate
400 immunofluorescence for both Kv2.1 and Kv2.2 on the apparent stem axons of DRG neurons (Figure 7 B,
401 D and E arrowheads, Figure 7-1). We observed Kv2 clusters on axons clearly protruding from C-fiber
402 neurons expressing soluble GFP (Figure 7-1 A), confirming stem axon localization.
403
404 While Kv2 clusters in central neurons and many DRG neurons are distributed evenly throughout the
405 soma, we found that DRG neurons asymmetrically distribute Kv2 clusters on the soma (Figure 7 B-E
406 arrows). To test if enrichment of Kv2 channel clusters is oriented to a specific region on the soma we
407 manually traced the surface of neurons whose apparent stem axons were visible (Figure 7 F). The
408 brightest anti-Kv2.1 and anti-Kv2.2 immunofluorescence is near the stem axon in 76 and 80% of DRG
409 neurons respectively (Figure 7 G and H). Asymmetric distribution of Kv2 channels is not frequently
410 observed in central neurons of mice (Bishop et al., 2018; Bishop et al., 2015; Romer et al., 2014)
411 suggesting a potentially unique role of Kv2 clusters in DRG neurons.
412

413 **Kv2.2 channels are expressed in peripheral axons of DRG neurons at the paranodes and**
414 **juxtaparanodes**
415
416 To determine if anti-Kv2 immunofluorescence is detectible in DRG axons in regions beyond the stem
417 axon we immunolabeled samples containing both peripheral and central axons, using NF200 or βIII
418 tubulin as a markers for DRG axons (Figure 8 and Figure 8-1). Neurons were not labeled with βIII tubulin
419 in Figure 8 because the βIII tubulin and Kv2.2 targeting antibodies were of the same isotype. We did not
420 observe anti-Kv2.1 immunofluorescence in peripheral axons (Figure 8-1) from neurons that did have
421 detectable anti-Kv2.1 immunofluorescence in the neuron soma (Figure 2). However, anti-Kv2.2
422 immunofluorescence is detectable in peripheral and central axons of WT but not Kv2.2 KO mice (Figure
423 8 B and C). Anti-Kv2.2 immunofluorescence on myelinated peripheral axons appears as discrete puncta
424 or as larger bands which span the width of the axon (Figure 8 B arrows). We also observed anti-Kv2.2
425 immunofluorescence not colocalized with NF200, suggestive of unmyelinated fibers (Figure 8 B
426 arrowhead). In MrgprD-GFP mice, anti-Kv2.2 immunofluorescence colocalizes with axons expressing
427 cytosolic GFP, identifying that unmyelinated C-fiber neurons also express Kv2.2 protein along the
428 peripheral axon (Figure 8 D)
429
430 We noted that anti-Kv2.2 immunofluorescence on myelinated fibers was not uniform and was in a
431 pattern suggestive of localization at nodes of Ranvier. To investigate if Kv2.2 channels have a nodal
432 subcellular localization we co-labeled peripheral axons with antibodies specific for CASPR (Einheber et
433 al., 1997) and Kv1.2 (Rasband et al., 1998) to identify the paranodal and juxtaparanodal regions of nodes
434 of Ranvier, respectively. We found punctate anti-Kv2.2 immunofluorescence associated with both the
435 paranode and juxtaparanode of WT DRG neuron axons that is not present in Kv2.2 KO mice (Figure 9 A).
436 We analyzed anti-Kv2.2 immunofluorescence at the paranode and juxtaparanode of WT and Kv2.2 KO

437 mice by manually drawing ROIs around CASPR and Kv1.2 immunofluorescence while blinded to anti-
438 Kv2.2 immunofluorescence and found that 26/34 paranodes and 20/31 juxtaparanodes had anti-Kv2.2
439 immunofluorescence brighter than the brightest anti-Kv2.2 immunofluorescence measured in the
440 paranodes and juxtaparanodes of Kv2.2 KO mice (Figure 9 B).
441
442 **Anti-Kv2.1 and anti-Kv2.2 immunofluorescence is non-uniform across DRG neuron subtypes**
443
444 DRG neurons are a highly heterogeneous population and different voltage gated potassium channel
445 families make distinct contributions to outward potassium currents in different sensory neuron subtypes
446 (Zheng et al., 2019). We observed subpopulations of DRG neurons that have bright anti-Kv2.1
447 immunofluorescence but dim anti-Kv2.2 immunofluorescence and vice-versa (Figure 10 A and C, Figure
448 1 A, and Figure 6 A). We hypothesized that the differences in the cellular expression patterns of Kv2.1
449 and Kv2.2 could potentially denote specific subtypes of sensory neurons. We assessed anti-Kv2.1 and
450 anti-Kv2.2 immunofluorescence in four DRG neuron subtypes, employing genetically encoded markers
451 for non-peptidergic nociceptors (MrgprD-GFP) or proprioceptors (PV-tdTomato), or immunolabeling to
452 mark peptidergic nociceptors (CGRP) or myelinated DRG neurons (NF200) (Figure 10 B and D). The
453 peptidergic and non-peptidergic nociceptors have similar ranges of both anti-Kv2.1 and anti-Kv2.2
454 immunofluorescence. Many neurons with the brightest anti-Kv2.1 or anti-Kv2.2 immunofluorescence
455 were NF200-positive myelinated neurons. Proprioceptors, a subset of the myelinated neurons, have a
456 range of anti-Kv2.2 but dim anti-Kv2.1 immunofluorescence. The neurons with bright anti-Kv2.1 and dim
457 anti-Kv2.2 immunofluorescence are mostly NF200-positive myelinated neurons of unknown subtype
458 (Figure 10 B and C). Overall, these results are consistent with mRNA transcript levels reported for Kv2.1
459 and Kv2.2 in DRG neuron subtypes; notably that Kv2.1 and Kv2.2 transcript levels are similar in identified

460 classes of DRG neurons, except for proprioceptors where Kv2.1 mRNA transcripts are low (Usoskin et al.,
461 2015; Zheng et al., 2019).
462
463
464 **Kv2 channel cellular expression and subcellular localization in human DRG neurons is similar to mice**
465
466 Previous work has shown that Kv2 mRNA transcripts are present in human DRG neurons (Tavares-
467 Ferreira et al., 2022; Wangzhou et al., 2020). As human Kv2.1 and Kv2.2 knockout controls are not
468 available, we compared fluorescence in DRG sections with anti-Kv2 primary antibodies to those lacking
469 primary antibodies to determine Kv2 channel protein localization in human DRG neurons. Control
470 samples lacking primary antibodies revealed strong autofluorescence at all excitation wavelengths
471 (Figure 11 A, Figure 11-1 A and B) consistent with other studies of human DRG neurons which have
472 attributed this autofluorescence to lipofuscin (Shiers et al., 2021). We found that most neurons have
473 anti-Kv2.1 and anti-Kv2.2 immunofluorescence brighter than controls lacking primary antibodies (Figure
474 11-1 D and E) suggesting that Kv2 protein is present in human DRG neurons. As a control, we used the
475 same methods with anti-Nav1.7 and anti-Nav1.8 antibodies and found anti-Nav1.7 immunofluorescence
476 in nearly all human DRG neurons while anti-Nav1.8 was in a smaller fraction of DRG neurons, consistent
477 with previous reports of Nav1.7 protein and Nav1.8 transcript in human DRG (Shiers, Klein, & Price,
478 2020) (Figure 11-1 A arrowheads, B, F and G). Similar to DRG neurons in mice, we observed
479 subpopulations of neurons that had bright anti-Kv2.1 immunofluorescence but low anti-Kv2.2
480 immunofluorescence and conversely neurons that had bright anti-Kv2.2 immunofluorescence but low
481 anti-Kv2.1 immunofluorescence (Figure 11 A and Figure 11-1 A and H). Attempts to label neurons with
482 antibodies that target parvalbumin were unsuccessful, and we were unable to identify if the population

483 of human DRG neurons with low anti-Kv2.1 and high anti-Kv2.2 are proprioceptors as we observed in
484 mice.
485
486 To identify if Kv2 protein subcellular localization in human is similar to mice we examined the pattern of
487 anti-Kv2.1 and anti-Kv2.2 immunofluorescence in sections of human DRG. We identified neurons in
488 human DRG where anti-Kv2.1 and anti-Kv2.2 immunofluorescence is enriched at the outer edge of DRG
489 neuron somata (Figure 11 A arrows and Figure 11-2). In some neurons, Kv2 clusters exhibited
490 asymmetric distribution on the neuronal soma (Figure 11 B arrows, Figure 11-2 arrows). *En face* z-
491 projections of human DRG neurons revealed Kv2 clusters as well as donut shapes similar to observations
492 in mice (Figure 11 C). We were not able to identify Kv2.1 on the stem axon of human DRG neurons but
493 did observe Kv2.2 on apparent stem axons (Figure 11 C arrow) along with anti-Nav1.7
494 immunofluorescence (Figure 11-3 arrow). To determine if Kv2.2 channels are present in human nodes of
495 Ranvier, we labeled human DRG sections with the same anti-Kv2.2, anti-CASPR and anti-Kv1.2 antibodies
496 that were used in mice. We found anti-Kv2.2 immunofluorescence at the CASPR-labeled paranode and
497 Kv1.2 labeled juxtaparanode of human DRG neuron fibers (Figure 11 D arrowheads and arrows
498 respectively) suggesting that these channels might contribute to electrical propagation or other
499 physiological functions in human DRG axons.
500
501 **DISSCUSSION**
502
503 Our results reveal overlapping yet distinct localization patterns of Kv2.1 and Kv2.2 in DRG neurons. Here,
504 we discuss the unique features of Kv2 localization in the DRG and how these could influence neuronal
505 physiology and somatosensation.
506

507 We identify differences between anti-Kv2.1 and anti-Kv2.2 immunofluorescence in DRG neurons. Kv2.2
508 mRNA is abundant in all DRG neuron subtypes identified, while Kv2.1 mRNA is low in proprioceptors and
509 abundant in other subtypes (Usoskin et al., 2015; Zheng et al., 2019). Consistent with these findings we
510 identify Kv2.1 and Kv2.2 immunofluorescence in most DRG neurons and find that Kv2.1
511 immunofluorescence is anomalously low in proprioceptors. Detection of Kv2.2 but not Kv2.1 in DRG
512 neuron peripheral and central axons suggests that Kv2.2 channels may be important for electrical
513 transmission in these axons. While detectable Kv2.2 remained constant in DRG neurons of older mice,
514 detectable Kv2.1 decreased, possibly contributing to the altered repolarization noted in DRG neurons
515 from aged mice (Scott, Leu, & Cinader, 1988). The differences between Kv2.1 and Kv2.2 in
516 somatosensory neurons are consistent with distinct roles for these Kv2 paralogs in somatosensory
517 neuron physiology, as seen in brain and pancreatic islets (Bishop et al., 2015; Johnston et al., 2008; Li et
518 al., 2013).
519
520 The expression and subcellular localization of Kv2 channels in DRG neurons are distinct from central
521 neurons. Kv2.1 is present in most brain neurons (Bishop et al., 2018; Bishop et al., 2015; Hwang, Fotuhi,
522 Bredt, Cunningham, & Snyder, 1993) while Kv2.2 is less broadly expressed (Bishop et al., 2015;
523 Hermanstyne et al., 2010; Hwang, Glatt, Bredt, Yellen, & Snyder, 1992; Johnston et al., 2008; Kihira et
524 al., 2010). In contrast to this, we find Kv2.2 is expressed in most if not all DRG neurons. We also identify
525 that Kv2.2 is enriched in the DRG relative to neurons in the spinal cord, suggesting that abundant Kv2.2
526 protein expression is a distinct feature of DRG neuron physiology. In central neurons, Kv2 channel
527 clusters are typically evenly distributed across neuron somata (Bishop et al., 2015; Kihira et al., 2010;
528 Muennich & Fyffe, 2004) and asymmetric subcellular localization of Kv2 clusters on neuron somata has
529 to our knowledge not been described. We find that Kv2 channels are enriched at the plasma membrane
530 in a subcellular region near the stem axon of some DRG neurons. Differences in Kv2 localization

531 between central neurons and the somatosensory neurons could arise from differences in the
532 extracellular environment surrounding DRG neuron somata. In central neurons, Kv2 channel clusters are
533 reported at cholinergic C-terminal synaptic sites, S-type synapses, and are apposed to astrocytic end
534 feet (Du et al., 1998; Muennich & Fyffe, 2004). However, synapses have not been reported in the DRG
535 and DRG neurons are surrounded by satellite glial cells instead of astrocytes (Matsuda et al., 2005).
536 Further studies could investigate if Kv2 clusters are localized to extracellular structures in the DRG. Kv2.2
537 has been identified in juxtaparanodes but not paranodes of axons in the osseous spiral lamina of the
538 cochlea (Kim & Rutherford, 2016) and previous work has also identified that Kv2.1 channels are
539 necessary for enabling ER Ca2+ uptake during electrical activity in both the soma and axon (Panzera et
540 al., 2022). To our knowledge, Kv2.2 channels have not been previously reported at the nodes of Ranvier
541 in the brain, spinal cord or DRG. Our results indicate that Kv2.2 channels are present at the
542 juxtaparanode and paranode of myelinated DRG neurons and also in the axons of unmyelinated DRG
543 neurons. The mechanism of Kv2.2 protein trafficking to the axon is unknown. Kv2.1 channels are
544 trafficked to the axon initial segment through a distinct secretory pathway (Jensen et al., 2017) allowing
545 neurons to regulate precise compartment specific localization of Kv2.1 protein. A similar mechanism for
546 Kv2.2 localization in DRG axons could allow neurons to independently control Kv2.2 protein expression
547 in the neuron soma and axon. The subcellular distribution of Kv2.1 and Kv2.2 subunits in DRG neurons
548 suggests they could each distinctly modulate electrical signals. We note that our observations could not
549 distinguish whether immunofluorescence in DRG axons could represent intracellular trafficking vesicles
550 of Kv2.2 proteins, or whether axonal Kv2.2 is on the membrane surface where it could modulate
551 electrical signals.
552
553 Kv2 channels in DRG neurons may play important roles in somatosensation and nociception. Kv2
554 conductances can modulate action potential repolarization, afterhyperpolarization and repetitive firing

555 (Liu & Bean, 2014; Zheng et al., 2019). Kv2 conductances modulate electrical transmission in rat DRG
556 neurons (Tsantoulas et al., 2014). Knockdown of Kv2.1 increases hypersensitivity to painful stimuli and
557 regulation of Kv2.1 protein expression through the epigenetic factor Cdyl modulates neuronal
558 excitability and nociception (Sun et al., 2022). Consistent with these studies, our results show that Kv2
559 channels are localized to DRG neuron axons, where they could potentially influence electrical
560 transmission.
561
562 Regulatory pore-forming subunits of the Kv5, Kv6, Kv8, and Kv9 "silent subunit" families obligately
563 assemble into heteromeric channels with Kv2 subunits (Bocksteins, 2016) and have been implicated in
564 nociception. Women with decreased sensitivity to labor pain were identified to have a mutation in the
565 Kv6.4 silent subunit that disrupts Kv2.1/Kv6.4 heteromer expression and is proposed to modulate
566 nociceptor signaling (Lee et al., 2020). Downregulation of the Kv9.1 silent subunit after axotomy evokes
567 hyperexcitability of DRG neurons (Tsantoulas et al., 2012). While both Kv2 channels are broadly
568 expressed in DRG neurons, transcript levels of silent subunits in mice and humans show much more
569 neuron subtype specificity (Tavares-Ferreira et al., 2022; Zheng et al., 2019), raising the possibility of
570 molecularly distinct Kv2-containing channels in somatosensory neuron subtypes.
571
572 Previous studies have identified that voltage gated ion channel expression can be substantially different
573 between mice and human DRG, notably, in the expression of Nav1.7 (Shiers et al., 2020). However, we
574 find expression of Kv2 channels to be similar in mouse and human DRG. An overall similarity is
575 supported by the presence of detectable Kv2 channels in most neurons, consistent with transcriptomics
576 data from both mice and humans (Tavares-Ferreira et al., 2022; Zheng et al., 2019). The subcellular
577 localization of Kv2 channels also appears similar between mice and humans. These similarities include
578 enrichment of Kv2 channels at the outer edge of neurons, Kv2 clusters on the neuron soma, and Kv2.2

579 on the stem axon, paranode and juxtaparanode. These similarities suggest that the functional roles of
580 Kv2 channels could be similar in both mouse and human DRG neurons.
581
582 Overall, we find attributes of Kv2 channel localization in somatosensory neurons that could point to
583 their functional roles in sensory information processing. The broad expression of Kv2.2 among DRG
584 neuron types and expansive axonal localization of Kv2.2 suggest a key role for this channel in the
585 somatosensory nervous system. The specialized divergence of Kv2.1 and Kv2.2 suggest the functional
586 roles of Kv2 subtypes in DRG neurons are overlapping yet distinct.

587 **REFERENCES**

588

589 Bishop, H. I., Cobb, M. M., Kirmiz, M., Parajuli, L. K., Mandikian, D., Philp, A. M., . . . Trimmer, J.
590 S. (2018). Kv2 ion channels determine the expression and localization of the associated
591 AMIGO-1 cell adhesion molecule in adult brain neurons. *Front Mol Neurosci, 11*, 1.
592 doi:10.3389/fnmol.2018.00001

593 Bishop, H. I., Guan, D., Bocksteins, E., Parajuli, L. K., Murray, K. D., Cobb, M. M., . . . Trimmer, J.
594 S. (2015). Distinct cell- and layer-specific expression patterns and independent
595 regulation of Kv2 channel subtypes in cortical pyramidal neurons. *J Neurosci, 35*(44),
596 14922-14942. doi:10.1523/jneurosci.1897-15.2015

597 Blaine, J. T., & Ribera, A. B. (1998). Heteromultimeric potassium channels formed by members
598 of the Kv2 subfamily. *J Neurosci, 18*(23), 9585-9593. doi:10.1523/jneurosci.18-23-
599 09585.1998

600 Bocksteins, E. (2016). Kv5, Kv6, Kv8, and Kv9 subunits: No simple silent bystanders. *J Gen*
601 *Physiol, 147*(2), 105-125. doi:10.1085/jgp.201511507

602 Bocksteins, E., Raes, A. L., Van de Vijver, G., Bruyns, T., Van Bogaert, P. P., & Snyders, D. J.
603 (2009). Kv2.1 and silent Kv subunits underlie the delayed rectifier K+ current in cultured
604 small mouse DRG neurons. *Am J Physiol Cell Physiol, 296*(6), C1271-1278.
605 doi:10.1152/ajpcell.00088.2009

606 Cho, W. G., & Valtschanoff, J. G. (2008). Vanilloid receptor TRPV1-positive sensory afferents in
607 the mouse ankle and knee joints. *Brain research, 1219*, 59-65.
608 doi:https://doi.org/10.1016/j.brainres.2008.04.043

Cotella, D., Hernandez-Enriquez, B., Wu, X., Li, R., Pan, Z., Leveille, J., . . . Sesti, F. (2012). Toxic role of K+ channel oxidation in mammalian brain. *J Neurosci, 32*(12), 4133-4144. doi:10.1523/jneurosci.6153-11.2012

Dirajlal, S., Pauers, L. E., & Stucky, C. L. (2003). Differential response properties of IB(4)-positive and -negative unmyelinated sensory neurons to protons and capsaicin. *J Neurophysiol, 89*(1), 513-524. doi:10.1152/jn.00371.2002

Dong, X., Han, S., Zylka, M. J., Simon, M. I., & Anderson, D. J. (2001). A diverse family of GPCRs expressed in specific subsets of nociceptive sensory neurons. *Cell, 106*(5), 619-632. doi:10.1016/s0092-8674(01)00483-4

Du, J., Tao-Cheng, J. H., Zerfas, P., & McBain, C. J. (1998). The K+ channel, Kv2.1, is apposed to astrocytic processes and is associated with inhibitory postsynaptic membranes in hippocampal and cortical principal neurons and inhibitory interneurons. *Neuroscience, 84*(1), 37-48. doi:https://doi.org/10.1016/S0306-4522(97)00519-8

Einheber, S., Zanazzi, G., Ching, W., Scherer, S., Milner, T. A., Peles, E., & Salzer, J. L. (1997). The axonal membrane protein Caspr, a homologue of neurexin IV, is a component of the septate-like paranodal junctions that assemble during myelination. *J Cell Biol, 139*(6), 1495-1506. doi:10.1083/jcb.139.6.1495

Fletcher, E. V., Simon, C. M., Pagiazitis, J. G., Chalif, J. I., Vukojicic, A., Drobac, E., . . . Mentis, G. Z. (2017). Reduced sensory synaptic excitation impairs motor neuron function via Kv2.1 in spinal muscular atrophy. *Nat Neurosci, 20*(7), 905-916. doi:10.1038/nn.4561

629 Gravagna, N. G., Knoeckel, C. S., Taylor, A. D., Hultgren, B. A., & Ribera, A. B. (2008). Localization
630 of Kv2.2 protein in Xenopus laevis embryos and tadpoles. *J Comp Neurol, 510*(5), 508-
631 524. doi:10.1002/cne.21804
632 Ha, H. (1970). Axonal bifurcation in the dorsal root ganglion of the cat: a light and electron
633 microscopic study. *J Comp Neurol, 140*(2), 227-240. doi:10.1002/cne.901400206
634 He, X. H., Zang, Y., Chen, X., Pang, R. P., Xu, J. T., Zhou, X., . . . Liu, X. G. (2010). TNF-α
635 contributes to up-regulation of Nav1.3 and Nav1.8 in DRG neurons following motor fiber
636 injury. *PAIN, 151*(2), 266-279. doi:10.1016/j.pain.2010.06.005
637 Hermanstyne, T. O., Kihira, Y., Misono, K., Deitchler, A., Yanagawa, Y., & Misonou, H. (2010).
638 Immunolocalization of the voltage-gated potassium channel Kv2.2 in GABAergic neurons
639 in the basal forebrain of rats and mice. *J Comp Neurol, 518*(21), 4298-4310.
640 doi:10.1002/cne.22457
641 Hwang, P. M., Fotuhi, M., Bredt, D. S., Cunningham, A. M., & Snyder, S. H. (1993). Contrasting
642 immunohistochemical localizations in rat brain of two novel K+ channels of the Shab
643 subfamily. *J Neurosci, 13*(4), 1569-1576. doi:10.1523/jneurosci.13-04-01569.1993
644 Hwang, P. M., Glatt, C. E., Bredt, D. S., Yellen, G., & Snyder, S. H. (1992). A novel K+ channel with
645 unique localizations in mammalian brain: molecular cloning and characterization.
646 *Neuron, 8*(3), 473-481. doi:10.1016/0896-6273(92)90275-i
647 Irie, T. (2021). Essential role of somatic Kv2 channels in high-frequency firing in cartwheel cells
648 of the dorsal cochlear nucleus. *eNeuro, 8*(3). doi:10.1523/eneuro.0515-20.2021
649 Jensen, C. S., Watanabe, S., Stas, J. I., Klaphaak, J., Yamane, A., Schmitt, N., . . . Misonou, H.
650 (2017). Trafficking of Kv2.1 channels to the axon initial segment by a novel

651 nonconventional secretory pathway. *J Neurosci, 37*(48), 11523-11536.
652 doi:10.1523/jneurosci.3510-16.2017
653 Johnson, B., Leek, A. N., Sole, L., Maverick, E. E., Levine, T. P., & Tamkun, M. M. (2018). Kv2
654 potassium channels form endoplasmic reticulum/plasma membrane junctions via
655 interaction with VAPA and VAPB. *Proc Natl Acad Sci U S A, 115*(31), E7331-e7340.
656 doi:10.1073/pnas.1805757115
657 Johnston, J., Griffin, S. J., Baker, C., Skrzypiec, A., Chernova, T., & Forsythe, I. D. (2008). Initial
658 segment Kv2.2 channels mediate a slow delayed rectifier and maintain high frequency
659 action potential firing in medial nucleus of the trapezoid body neurons. *J Physiol,*
660 *586*(14), 3493-3509. doi:10.1113/jphysiol.2008.153734
661 Kihira, Y., Hermanstyne, T. O., & Misonou, H. (2010). Formation of heteromeric Kv2 channels in
662 mammalian brain neurons. *J Biol Chem, 285*(20), 15048-15055.
663 doi:10.1074/jbc.M109.074260
664 Kim, K. X., & Rutherford, M. A. (2016). Maturation of NaV and Kv channel topographies in the
665 auditory nerve spike initiator before and after developmental onset of hearing function.
666 *J Neurosci, 36*(7), 2111-2118. doi:10.1523/jneurosci.3437-15.2016
667 King, A. N., Manning, C. F., & Trimmer, J. S. (2014). A unique ion channel clustering domain on
668 the axon initial segment of mammalian neurons. *J Comp Neurol, 522*(11), 2594-2608.
669 doi:10.1002/cne.23551
670 Kirmiz, M., Vierra, N. C., Palacio, S., & Trimmer, J. S. (2018). Identification of VAPA and VAPB as
671 Kv2 channel-interacting proteins defining endoplasmic reticulum-plasma membrane
672 junctions in mammalian brain neurons. *J Neurosci*. doi:10.1523/jneurosci.0893-18.2018

Lee, M. C., Nahorski, M. S., Hockley, J. R. F., Lu, V. B., Ison, G., Pattison, L. A., . . . Woods, C. G. (2020). Human labor pain is influenced by the voltage-gated potassium channel Kv 6.4 subunit. *Cell Rep, 32*(3), 107941. doi:10.1016/j.celrep.2020.107941

Legland, D., Arganda-Carreras, I., & Andrey, P. (2016). MorphoLibJ: integrated library and plugins for mathematical morphology with ImageJ. *Bioinformatics, 32*(22), 3532-3534. doi:10.1093/bioinformatics/btw413

Li, X. N., Herrington, J., Petrov, A., Ge, L., Eiermann, G., Xiong, Y., . . . Zhou, Y. P. (2013). The role of voltage-gated potassium channels Kv2.1 and Kv2.2 in the regulation of insulin and somatostatin release from pancreatic islets. *J Pharmacol Exp Ther, 344*(2), 407-416. doi:10.1124/jpet.112.199083

Lim, S. T., Antonucci, D. E., Scannevin, R. H., & Trimmer, J. S. (2000). A novel targeting signal for proximal clustering of the Kv2.1 K+ channel in hippocampal neurons. *Neuron, 25*(2), 385-397. doi:10.1016/s0896-6273(00)80902-2

Liu, P. W., & Bean, B. P. (2014). Kv2 channel regulation of action potential repolarization and firing patterns in superior cervical ganglion neurons and hippocampal CA1 pyramidal neurons. *J Neurosci, 34*(14), 4991-5002. doi:10.1523/jneurosci.1925-13.2014

Matsuda, S., Kobayashi, N., Terashita, T., Shimokawa, T., Shigemoto, K., Mominoki, K., . . . Fujiwara, T. (2005). Phylogenetic investigation of Dogiel's pericellular nests and Cajal's initial glomeruli in the dorsal root ganglion. *J Comp Neurol, 491*(3), 234-245. doi:10.1002/cne.20713

Misonou, H., Mohapatra, D. P., Menegola, M., & Trimmer, J. S. (2005). Calcium- and metabolic state-dependent modulation of the voltage-dependent Kv2.1 channel regulates

neuronal excitability in response to ischemia. *J Neurosci, 25*(48), 11184-11193. doi:10.1523/jneurosci.3370-05.2005

Muennich, E. A., & Fyffe, R. E. (2004). Focal aggregation of voltage-gated, Kv2.1 subunit-containing, potassium channels at synaptic sites in rat spinal motoneurones. *J Physiol, 554*(Pt 3), 673-685. doi:10.1113/jphysiol.2003.056192

Newkirk, G. S., Guan, D., Dembrow, N., Armstrong, W. E., Foehring, R. C., & Spain, W. J. (2022). Kv2.1 potassium channels regulate repetitive burst firing in extratelencephalic neocortical pyramidal neurons. *Cereb Cortex, 32*(5), 1055-1076. doi:10.1093/cercor/bhab266

Panzera, L. C., Johnson, B., Quinn, J. A., Cho, I. H., Tamkun, M. M., & Hoppa, M. B. (2022). Activity-dependent endoplasmic reticulum Ca(2+) uptake depends on Kv2.1-mediated endoplasmic reticulum/plasma membrane junctions to promote synaptic transmission. *Proc Natl Acad Sci U S A, 119*(30), e2117135119. doi:10.1073/pnas.2117135119

Park, K. S., Mohapatra, D. P., Misonou, H., & Trimmer, J. S. (2006). Graded regulation of the Kv2.1 potassium channel by variable phosphorylation. *Science, 313*(5789), 976-979. doi:10.1126/science.1124254

Rasband, M. N., Trimmer, J. S., Schwarz, T. L., Levinson, S. R., Ellisman, M. H., Schachner, M., & Shrager, P. (1998). Potassium channel distribution, clustering, and function in remyelinating rat axons. *J Neurosci, 18*(1), 36-47. doi:10.1523/jneurosci.18-01-00036.1998

715 Regnier, G., Bocksteins, E., Van de Vijver, G., Snyders, D. J., & van Bogaert, P. P. (2016). The
716 contribution of Kv2.2-mediated currents decreases during the postnatal development of
717 mouse dorsal root ganglion neurons. *Physiol Rep, 4*(6). doi:10.14814/phy2.12731
718 Romer, S. H., Dominguez, K. M., Gelpi, M. W., Deardorff, A. S., Tracy, R. C., & Fyffe, R. E. W.
719 (2014). Redistribution of Kv2.1 ion channels on spinal motoneurons following peripheral
720 nerve injury. *Brain research, 1547*, 1-15. doi:10.1016/j.brainres.2013.12.012
721 Sarmiere, P. D., Weigle, C. M., & Tamkun, M. M. (2008). The Kv2.1 K+ channel targets to the
722 axon initial segment of hippocampal and cortical neurons in culture and in situ. *BMC*
723 *Neurosci, 9*, 112. doi:10.1186/1471-2202-9-112
724 Scannevin, R. H., Murakoshi, H., Rhodes, K. J., & Trimmer, J. S. (1996). Identification of a
725 cytoplasmic domain important in the polarized expression and clustering of the Kv2.1 K+
726 channel. *J Cell Biol, 135*(6 Pt 1), 1619-1632. doi:10.1083/jcb.135.6.1619
727 Schindelin, J., Arganda-Carreras, I., Frise, E., Kaynig, V., Longair, M., Pietzsch, T., . . . Cardona, A.
728 (2012). Fiji: an open-source platform for biological-image analysis. *Nat Methods, 9*(7),
729 676-682. doi:10.1038/nmeth.2019
730 Scott, B., Leu, J., & Cinader, B. (1988). Effects of aging on neuronal electrical membrane
731 properties. *Mech Ageing Dev, 44*(3), 203-214. doi:10.1016/0047-6374(88)90022-x
732 Shields, S. D., Ahn, H. S., Yang, Y., Han, C., Seal, R. P., Wood, J. N., . . . Dib-Hajj, S. D. (2012).
733 Nav1.8 expression is not restricted to nociceptors in mouse peripheral nervous system.
734 *PAIN, 153*(10), 2017-2030. doi:10.1016/j.pain.2012.04.022

735 Shiers, S., Klein, R. M., & Price, T. J. (2020). Quantitative differences in neuronal subpopulations
736 between mouse and human dorsal root ganglia demonstrated with RNAscope in situ
737 hybridization. *PAIN, 161*(10), 2410-2424. doi:10.1097/j.pain.0000000000001973
738 Shiers, S., Sankaranarayanan, I., Jeevakumar, V., Cervantes, A., Reese, J. C., & Price, T. J. (2021).
739 Convergence of peptidergic and non-peptidergic protein markers in the human dorsal
740 root ganglion and spinal dorsal horn. *J Comp Neurol, 529*(10), 2771-2788.
741 doi:10.1002/cne.25122
742 Sun, Z. W., Waybright, J. M., Beldar, S., Chen, L., Foley, C. A., Norris-Drouin, J. L., . . . Wang, Y.
743 (2022). Cdyl deficiency brakes neuronal excitability and nociception through promoting
744 Kcnb1 transcription in peripheral sensory neurons. *Adv Sci (Weinh), 9*(10), e2104317.
745 doi:10.1002/advs.202104317
746 Tavares-Ferreira, D., Shiers, S., Ray, P. R., Wangzhou, A., Jeevakumar, V., Sankaranarayanan, I., .
747 . . Price, T. J. (2022). Spatial transcriptomics of dorsal root ganglia identifies molecular
748 signatures of human nociceptors. *Sci Transl Med, 14*(632), eabj8186.
749 doi:10.1126/scitranslmed.abj8186
750 Thapa, P., Stewart, R., Sepela, R. J., Vivas, O., Parajuli, L. K., Lillya, M., . . . Sack, J. T. (2021).
751 EVAP: A two-photon imaging tool to study conformational changes in endogenous Kv2
752 channels in live tissues. *J Gen Physiol, 153*(11). doi:10.1085/jgp.202012858
753 Trimmer, J. S. (1991). Immunological identification and characterization of a delayed rectifier K+
754 channel polypeptide in rat brain. *Proc Natl Acad Sci U S A, 88*(23), 10764-10768.
755 doi:10.1073/pnas.88.23.10764

Tsantoulas, C., Zhu, L., Shaifta, Y., Grist, J., Ward, J. P., Raouf, R., . . . McMahon, S. B. (2012). Sensory neuron downregulation of the Kv9.1 potassium channel subunit mediates neuropathic pain following nerve injury. *J Neurosci, 32*(48), 17502-17513. doi:10.1523/jneurosci.3561-12.2012

Tsantoulas, C., Zhu, L., Yip, P., Grist, J., Michael, G. J., & McMahon, S. B. (2014). Kv2 dysfunction after peripheral axotomy enhances sensory neuron responsiveness to sustained input. *Exp Neurol, 251*, 115-126. doi:10.1016/j.expneurol.2013.11.011

Usoskin, D., Furlan, A., Islam, S., Abdo, H., Lönnerberg, P., Lou, D., . . . Ernfors, P. (2015). Unbiased classification of sensory neuron types by large-scale single-cell RNA sequencing. *Nat Neurosci, 18*(1), 145-153. doi:10.1038/nn.3881

Valtcheva, M. V., Copits, B. A., Davidson, S., Sheahan, T. D., Pullen, M. Y., McCall, J. G., . . . Gereau, R. W. t. (2016). Surgical extraction of human dorsal root ganglia from organ donors and preparation of primary sensory neuron cultures. *Nat Protoc, 11*(10), 1877-1888. doi:10.1038/nprot.2016.111

Vierra, N. C., O'Dwyer, S. C., Matsumoto, C., Santana, L. F., & Trimmer, J. S. (2021). Regulation of neuronal excitation-transcription coupling by Kv2.1-induced clustering of somatic L-type Ca(2+) channels at ER-PM junctions. *Proc Natl Acad Sci U S A, 118*(46). doi:10.1073/pnas.2110094118

Vullhorst, D., Mitchell, R. M., Keating, C., Roychowdhury, S., Karavanova, I., Tao-Cheng, J. H., & Buonanno, A. (2015). A negative feedback loop controls NMDA receptor function in cortical interneurons via neuregulin 2/ErbB4 signalling. *Nat Commun, 6*, 7222. doi:10.1038/ncomms8222

Wang, H., & Zylka, M. J. (2009). Mrgprd-expressing polymodal nociceptive neurons innervate most known classes of substantia gelatinosa neurons. *J Neurosci, 29*(42), 13202-13209. doi:10.1523/jneurosci.3248-09.2009

Wangzhou, A., McIlvried, L. A., Paige, C., Barragan-Iglesias, P., Shiers, S., Ahmad, A., . . . Price, T. J. (2020). Pharmacological target-focused transcriptomic analysis of native vs cultured human and mouse dorsal root ganglia. *PAIN, 161*(7), 1497-1517. doi:10.1097/j.pain.0000000000001866

Zheng, Y., Liu, P., Bai, L., Trimmer, J. S., Bean, B. P., & Ginty, D. D. (2019). Deep sequencing of somatosensory neurons reveals molecular determinants of intrinsic physiological properties. *Neuron, 103*(4), 598-616.e597. doi:10.1016/j.neuron.2019.05.039

Figure 1

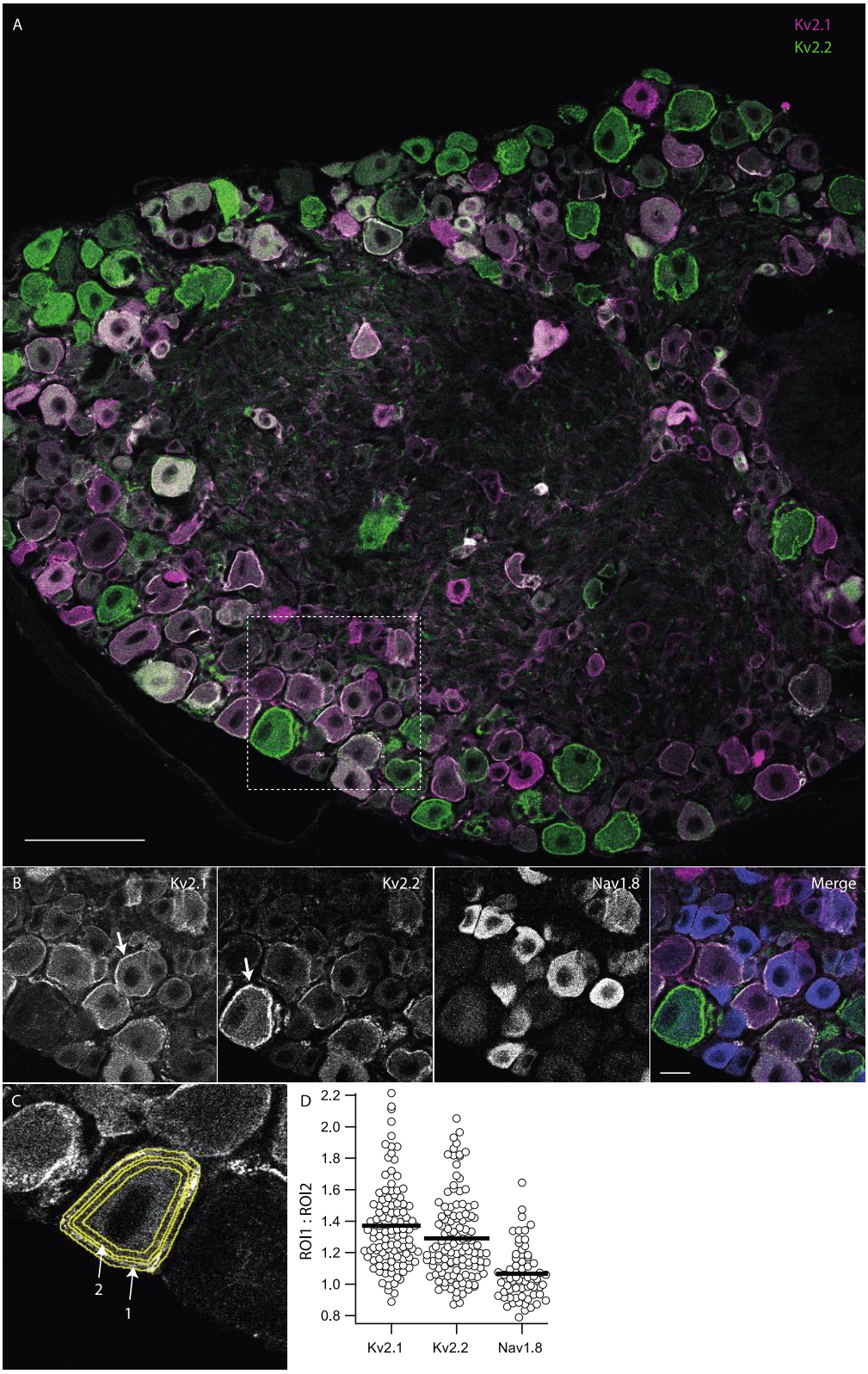
A
Kv2.1
Kv2.2
B
Kv2.1
Kv2.2
Nav1.8
Merge
C
2
1
D
ROI1 : ROI2
2.2
2.0
1.8
1.6
1.4
1.2
1.0
0.8
Kv2.1
Kv2.2
Nav1.8

791 **Figure 1 legend**

792 Kv2.1 and Kv2.2 protein are enriched at the outer edge of DRG neuron somas relative to
793 Nav1.8. Lumbar DRG section from an 11 week old male mouse labeled with antibodies which
794 target Kv2.1, Kv2.2 or Nav1.8. ***A***, Anti-Kv2.1 (magenta) and anti-Kv2.2 (green)
795 immunofluorescence in a lumbar DRG section. Scale bar is 100 µm. ***B***, Anti-Kv2.1, anti-Kv2.2 and
796 anti-Nav1.8 immunofluorescence from box shown in A. Arrows indicate prominent localization
797 of anti-Kv2 immunofluorescence at the edge of DRG neuron somas. In merge image anti-Kv2.1,
798 anti-Kv2.2 and anti-Nav1.8 immunofluorescence is magenta, green and blue respectively. Scale
799 bar is 20 µm. ***C***, Representative ROIs that encompass the outer edge of DRG neurons (arrow 1)
800 and the region just inside the outer edge (arrow 2). ***D***, Ratio of anti-Kv2.1, anti-Kv2.2 or anti-
801 Nav1.8 immunofluorescence from outer and inner ROIs for individual neurons from image in A.
802 Bars represent mean.

803

Figure 2

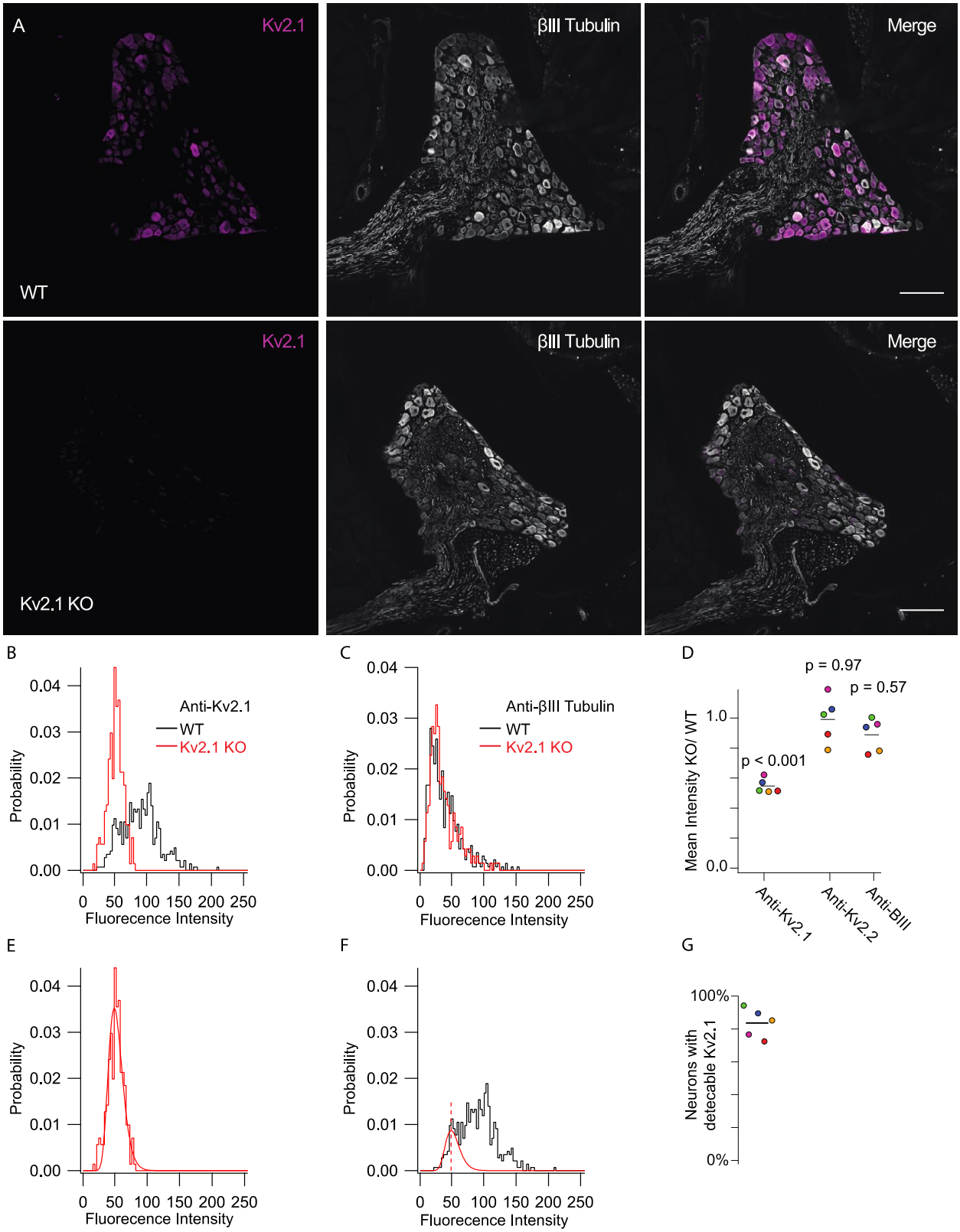
A
Kv2.1
βIII Tubulin
Merge
WT
Kv2.1
βIII Tubulin
Merge
Kv2.1 KO
B
Anti-Kv2.1
WT
Kv2.1 KO
Probability
Fluorecence Intensity
C
Anti-βIII Tubulin
WT
Kv2.1 KO
Probability
Fluorecence Intensity
D
p = 0.97
p = 0.57
p < 0.001
Mean Intensity KO/ WT
Anti-Kv2.1
Anti-Kv2.2
Anti-BIII
E
Probability
Fluorecence Intensity
F
Probability
Fluorecence Intensity
G
Neurons with detecable Kv2.1
100%
0%

806 **Figure 2 legend**

807 Kv2.1 protein is detectable in most mouse DRG neurons. ***A***, WT (top) and Kv2.1 KO (bottom)
808 DRG sections immunolabeled for Kv2.1 (magenta) and BIII tubulin (white). Images were taken
809 with identical imaging settings and are set to the same brightness and contrast. Scale bars are
810 100 µm. ***B***, Distribution of fluorescence intensity from WT (black) and Kv2.1 KO (red) neurons.
811 Data represent fluorescence intensity of 476 WT neurons from 10 DRG sections from 1 mouse
812 or 235 Kv2.1 KO neurons from 5 DRG sections from 1 mouse. DRG sections were taken from 7
813 week old female mice and are from the 13th thoracic DRG. Images shown in A represent one
814 section from WT and Kv2.1 KO mice used in this data set. ***C***, Distribution of BIII tubulin -
815 fluorescence intensity from the same WT (black) and Kv2.1 KO (red) neurons shown in B. ***D***,
816 Mean fluorescence intensity of Kv2.1 KO neurons normalized to WT neurons labeled with anti-
817 Kv2.1, anti-Kv2.2 and anti-BIII tubulin antibodies. Each point represents one Kv2.1 KO mouse
818 normalized to one age and sex matched WT mouse which was stained simultaneously and
819 imaged with identical microscopy settings. The color of each point represents the same mouse
820 and purple points represent data from the mouse whose DRG immunofluorescence data are
821 shown in A, B and C. p-values are calculated by a Students T-test and compares if points have a
822 significant difference from 1. ***E***, Kv2.1 KO data shown in B fit with a log normal distribution (red
823 fit). ***F***, WT data shown in B fit with the Kv2.1 KO distribution (red fit) where width and mean
824 were constrained to the Kv2.1 KO distribution and amplitude was unconstrained (equation 1).
825 Red dotted line represents the mean of the Kv2.1 KO distribution. Only WT data to the left of
826 red dotted line was used for the fit. ***G***, Percent of neurons with detectable Kv2.1 protein of 5

827 mice (1 female and 4 males). Point colors correspond to the WT mice analyzed in D. All mice

828 were compared to age and sex matched Kv2.1 KO mice.

Figure 3

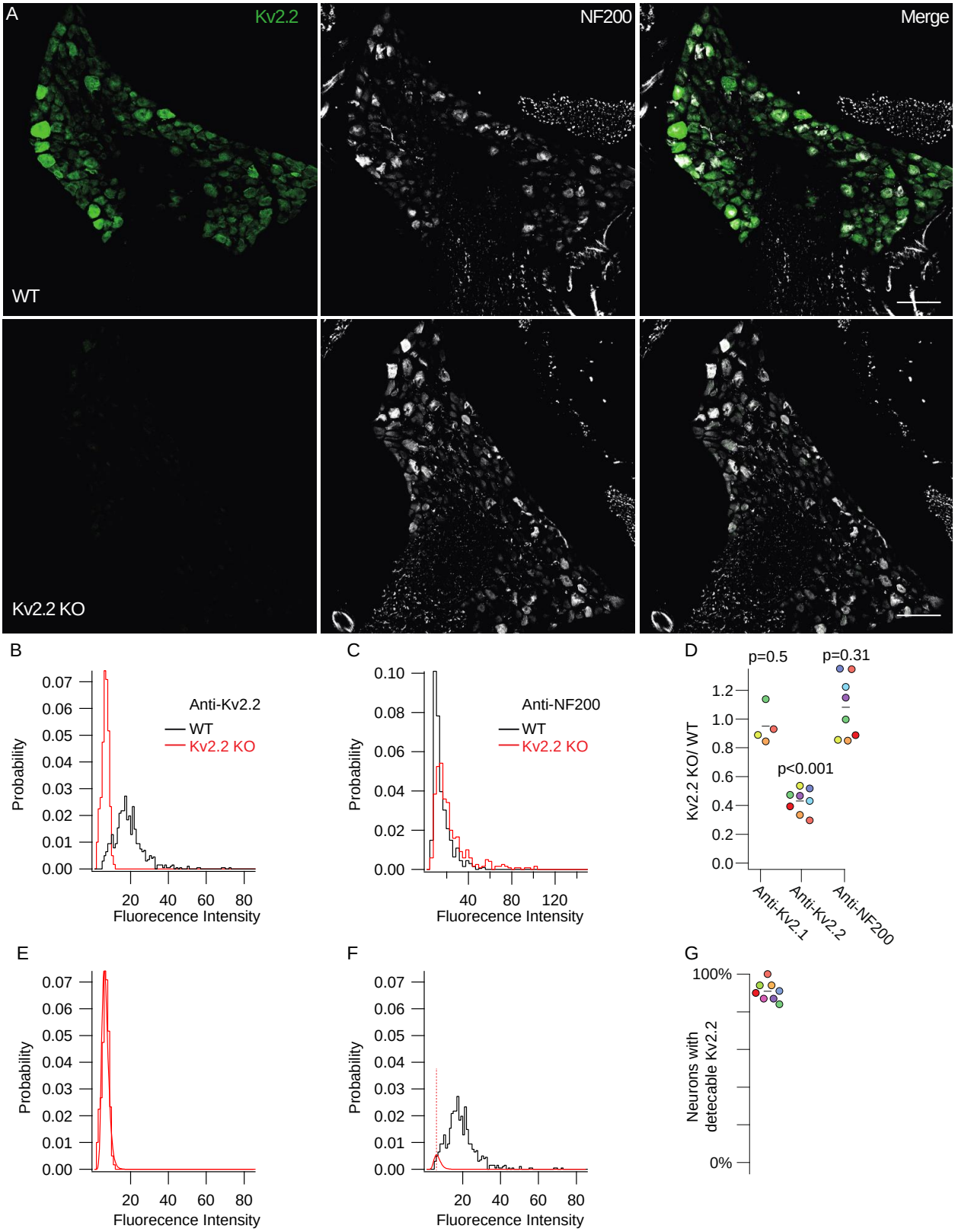
A
Kv2.2
NF200
Merge
WT
Kv2.2 KO
B
Probability
Anti-Kv2.2
WT
Kv2.2 KO
Fluorecence Intensity
C
Anti-NF200
WT
Kv2.2 KO
Fluorecence Intensity
D
p=0.5
p=0.31
p<0.001
Kv2.2 KO/ WT
Anti-Kv2.1
Anti-Kv2.2
Anti-NF200
E
Probability
Fluorecence Intensity
F
Probability
Fluorecence Intensity
G
100%
0%
Neurons with detecable Kv2.2

831 **Figure 3 legend**

832 Detectable Kv2.2 protein is present in most if not all mouse DRG neurons. ***A***, WT (top) and
833 Kv2.2 KO (bottom) DRG sections from the 13th thoracic DRG in 7 week old male mice
834 immunolabeled for Kv2.2 (green) and NF200 (white). Identical imaging and display settings.
835 Scale bars are 100 µm. **B**, Distribution of fluorescence intensities from WT (black) and Kv2.2 KO
836 (red) neurons. 672 WT neurons from 1 mouse. 398 Kv2.2 KO neurons from 1 mouse. Data from
837 same mice shown in A. ***C***, Distribution of anti-NF200 immunofluorescence intensity from the
838 same WT (black) and Kv2.2 KO (red) neurons shown in B. ***D***, Mean fluorescence intensity of
839 Kv2.2 KO neurons normalized to WT neurons labeled with anti-Kv2.1, anti-Kv2.2 and anti-NF200
840 antibodies. Each point represents one Kv2.2 KO mouse normalized to one age and sex matched
841 WT mouse which was stained simultaneously and imaged with identical microscopy settings.
842 The color of each point represents the same mouse and purple points represent data from the
843 male mouse whose DRG immunofluorescence data are shown in A, B and C. Missing points in
844 anti-Kv2.1 column are because some sections were not labeled with anti-Kv2.1 antibodies. p-
845 values are calculated by a Students T-test and compares if points have a significant difference
846 from 1. ***E***, Kv2.2 KO data shown in B fit with a log normal distribution (red fit). ***F***, WT data shown
847 in B fit with the Kv2.2 KO distribution (red fit) where width and mean were constrained to the
848 Kv2.2 KO distribution and amplitude was unconstrained (equation 1). Red dotted line
849 represents the mean of the Kv2.2 KO distribution. Only WT data to the left of red dotted line
850 was used for the fit. **G**, Percent of neurons with detectable Kv2.2 protein of 8 mice (7 males and

851 1 female). Point colors correspond to the WT mice analyzed in D. All mice were compared to

852 age and sex matched Kv2.2 KO mice.

853

854 **Figure 4**

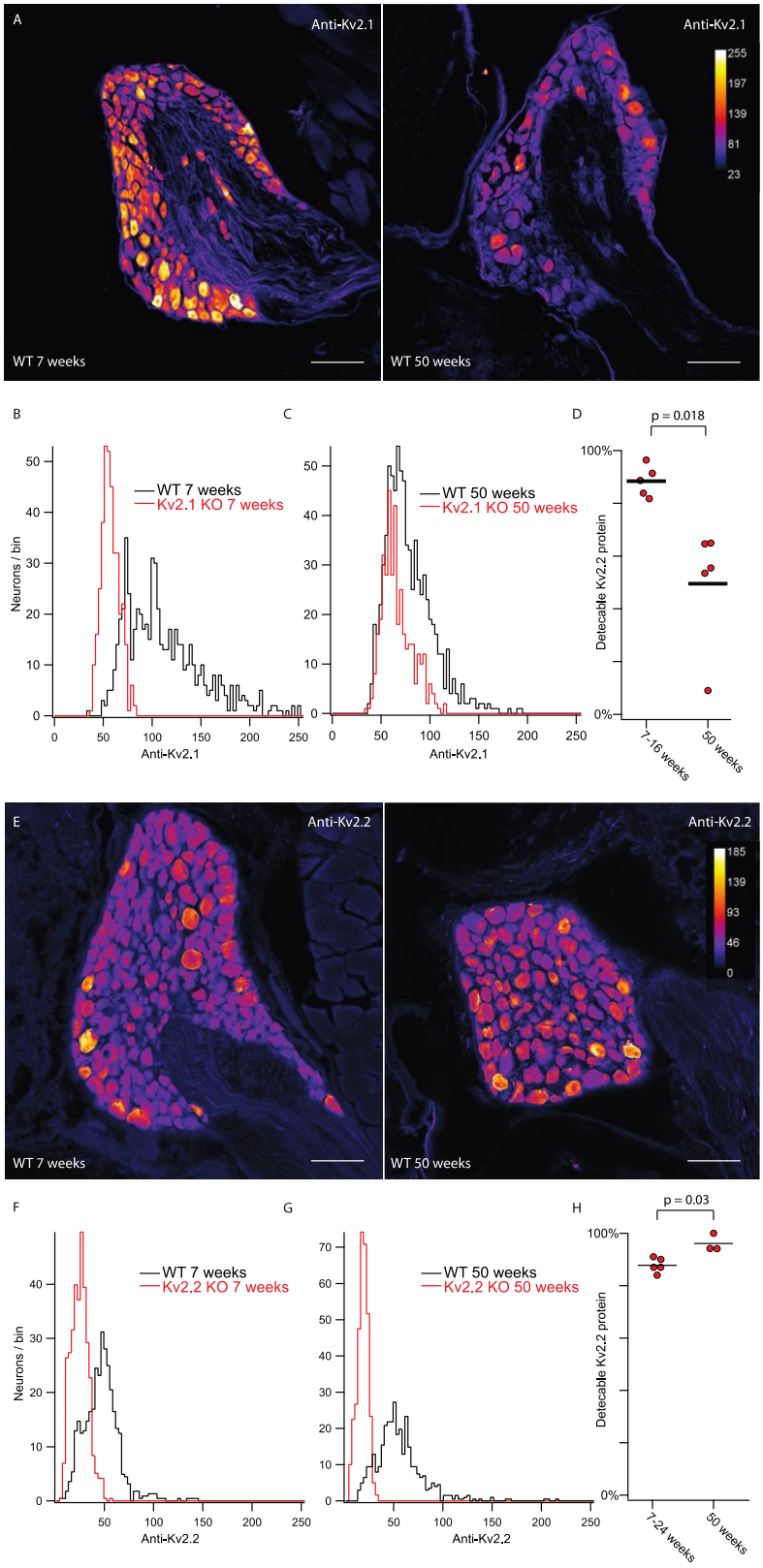

855

856 **Figure 4 legend**

857 Detectable Kv2.1 protein decreases in older mice while detectable Kv2.2 does not. ***A***, DRG
858 sections from the 13th thoracic DRG in 7 week (left) and 50 week (right) old mice
859 immunolabeled for Kv2.1. Vertical bar on right is pseudo coloring key for pixel intensity.
860 Identical imaging and display settings. Scale bars are 100 µm. ***B***, Distribution of fluorescence
861 intensities from 7 week old WT (black) and 7 week old Kv2.1 KO (red) neurons. 609 WT neurons
862 from 1 mouse. 367 Kv2.1 KO neurons from 1 mouse. ***C***, Distribution of fluorescence intensities
863 from 50 week old WT (black) and 50 week old Kv2.1 KO (red) neurons. 793 WT neurons from 1
864 mouse. 378 Kv2.1 KO neurons from 1 mouse. ***D***, Percent of neurons with detectable Kv2.1
865 protein in 7-16 week old and 50 week old mice. Data from 7-16 week old mice is the same data
866 in Figure 2. ***E***, DRG sections from the 13th thoracic DRG in 7 week (left) and 50 week (right) old
867 mice immunolabeled for Kv2.2. Vertical bar on right is pseudo coloring key for pixel intensity.
868 Identical imaging and display settings. Scale bars are 100 µm. ***F***, Distribution of fluorescence
869 intensities from 7 week old WT (black) and 7 week old Kv2.2 KO (red) neurons. 746 WT neurons
870 from 1 mouse. 717 Kv2.2 KO neurons from 1 mouse. Data from same mice shown in E. ***G***,
871 Distribution of fluorescence intensities from 50 week old WT (black) and 50 week old Kv2.2 KO
872 (red) neurons. 671 WT neurons from 1 mouse. 398 Kv2.2 KO neurons from 1 mouse. Data from
873 same mice shown in E. ***H***, Percent of neurons with detectable Kv2.2 protein in 7-24 week old
874 and 50 week old mice. Data is the same data from Figure 3 where mice were separated into a
875 young group (7-24 weeks) and an old group (50 weeks).

876

877

878 **Figure 5**

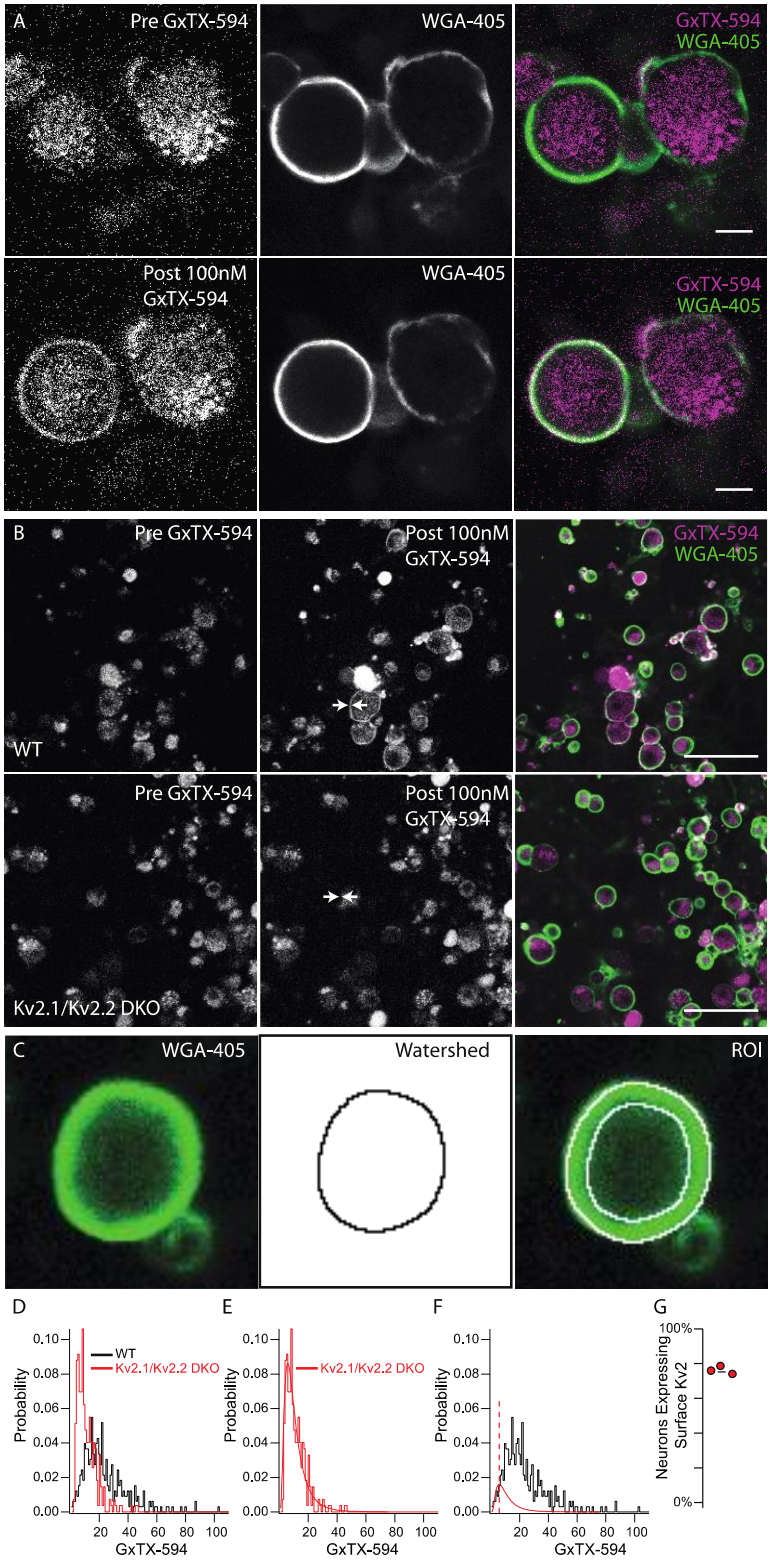

879

880 **Figure 5 legend**

881 Kv2 channels are expressed at the surface membrane of DRG neurons. ***A***, Fluorescence of live
882 dissociated DRG neurons excited at 594 nm before (top left) and after (bottom left) application
883 of 100 nM GxTX-594. Fluorescence from membrane marker WGA-405 before (top middle) and
884 after application of 100 nM GxTX-594 (bottom middle). Merge image shows 594 excitation
885 fluorescence (magenta) and 405 excitation fluorescence (green). Scale bar 20 µm. ***B***,
886 Dissociated DRG neurons from WT (top) and Kv2.1/Kv2.2 DKO (bottom) mice before and after
887 the application of GxTX-594, left panel and middle panel respectively. Arrows in middle panel
888 indicate location of soma membrane based on WGA-405 fluorescence. Right images are merge
889 of 594 excitation fluorescence (magenta) and 405 excitation fluorescence (green) after
890 application of 100 nM GxTX-594. Scale bars 100 µm. ***C***, Example of WGA-405 fluorescence (left)
891 used in watershed segmentation (middle) to generate annulus ROI (right) used to analyze
892 fluorescence intensity at the membrane. ***D***, Distribution of fluorescence intensity from WT
893 (black) and Kv2.1/Kv2.2 DKO (red) neurons. Data represents the fluorescence intensity of 326
894 WT neurons from 1 mouse or 271 Kv2.1/Kv2.2 DKO neurons from 1 mouse. DRG from all levels
895 of the spinal cord were pooled. ***E***, Kv2.1/Kv2.2 DKO data shown in D fit with a log normal
896 distribution (red fit). ***F***, WT data shown in D fit with the Kv2.1/Kv2.2 DKO distribution (red fit)
897 where width and mean were constrained to the Kv2.1/Kv2.2 DKO distribution and amplitude
898 was unconstrained (equation 1). Red dotted line represents the mean of the Kv2.1/Kv2.2 DKO
899 distribution. Only WT data to the left of red dotted line was used for the fit. ***G***, Percent of
900 neurons with detectable surface Kv2 protein, from an experiment where one WT mouse was

901 compared to one DKO mouse and an identical experiment where two WT mice were compared

902 to one DKO mouse (N=3 WT mice N=2 Kv2.1/Kv2.2 DKO mice).

903 **Figure 6**

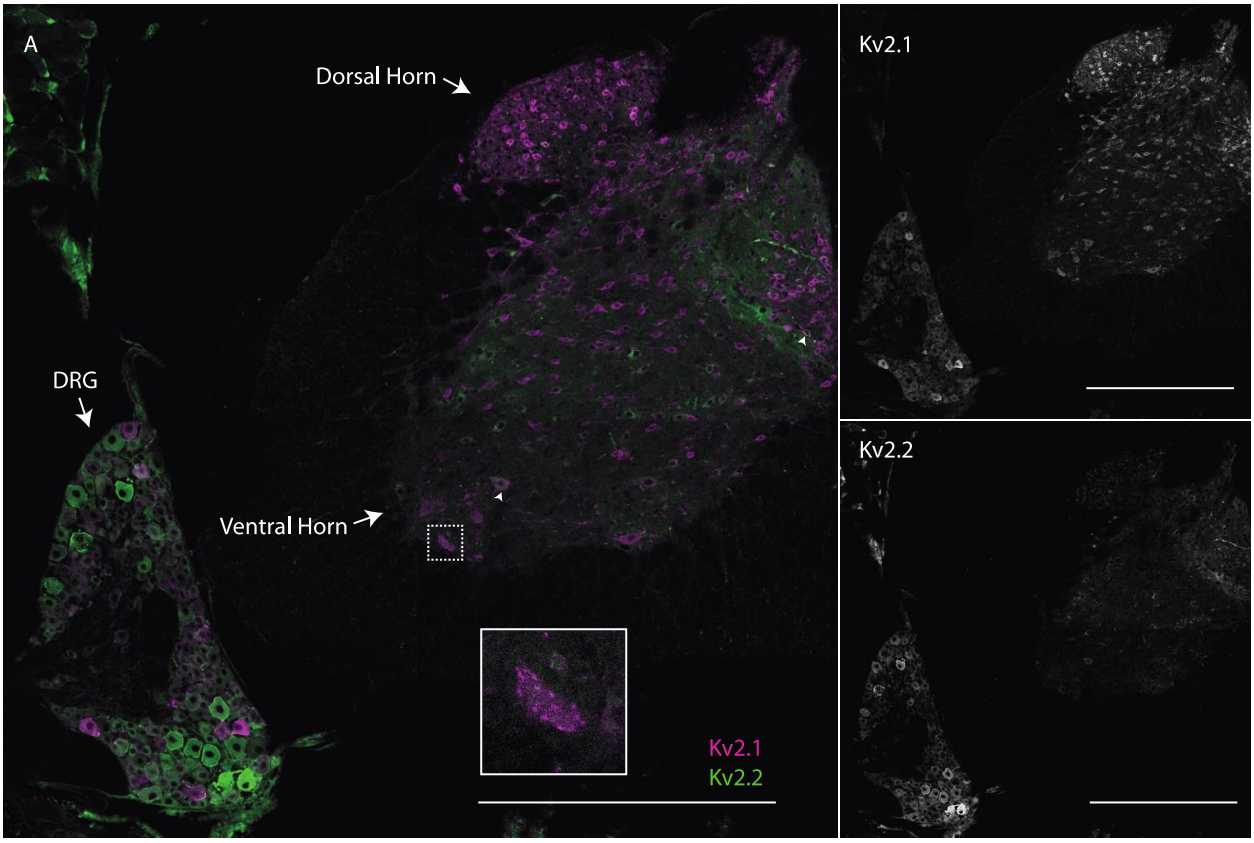

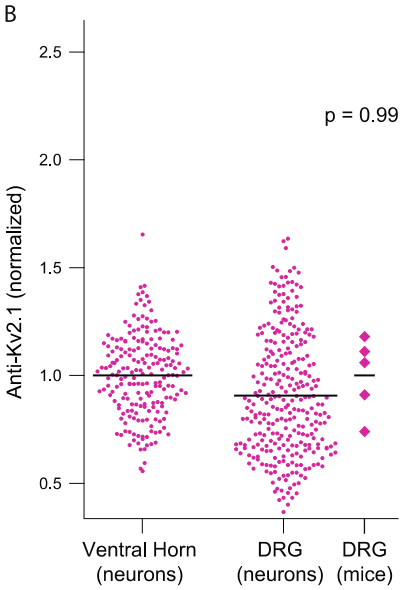

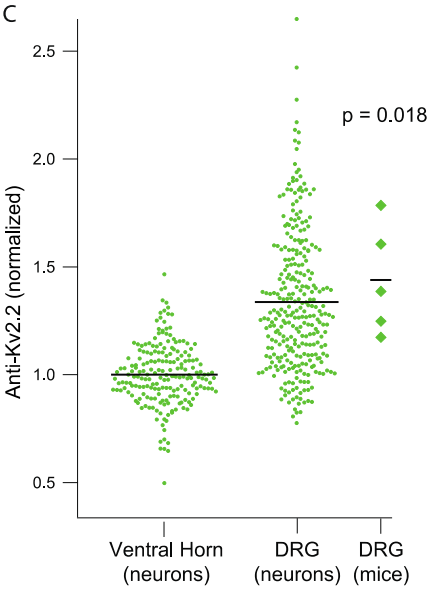

904

905 **Figure 6 legend**

906 DRG neurons have enriched Kv2.2 protein compared to neurons in the spinal cord. ***A***, Anti-
907 Kv2.1 (magenta) and anti-Kv2.2 (green) immunofluorescence in a spinal cord section from the
908 2nd lumbar vertebra (left). Anti-Kv2.1 immunofluorescence (right top) and anti-Kv2.2
909 immunofluorescence (right bottom). Arrows show neurons in the spinal cord with punctate
910 anti-Kv2.1 immunofluorescence. Arrow heads show neurons in the spinal cord with anti-Kv2.2
911 immunofluorescence. Scale bars are 500 µm. ***B***, Anti-Kv2.1 immunofluorescence from individual
912 neurons (circles) in the DRG and ventral horn normalized to the average fluorescence intensity
913 of neurons in the ventral horn. Diamonds to the right of data represent the average intensity in
914 DRG neurons of individual mice. Significant differences from 1 were calculated for individual
915 mice using Students t-test. N = 5 mice n = 295 in DRG and n = 200 in ventral horn. ***C***, Identical
916 analysis shown in B with anti-Kv2.2 immunofluorescence.

Figure 7

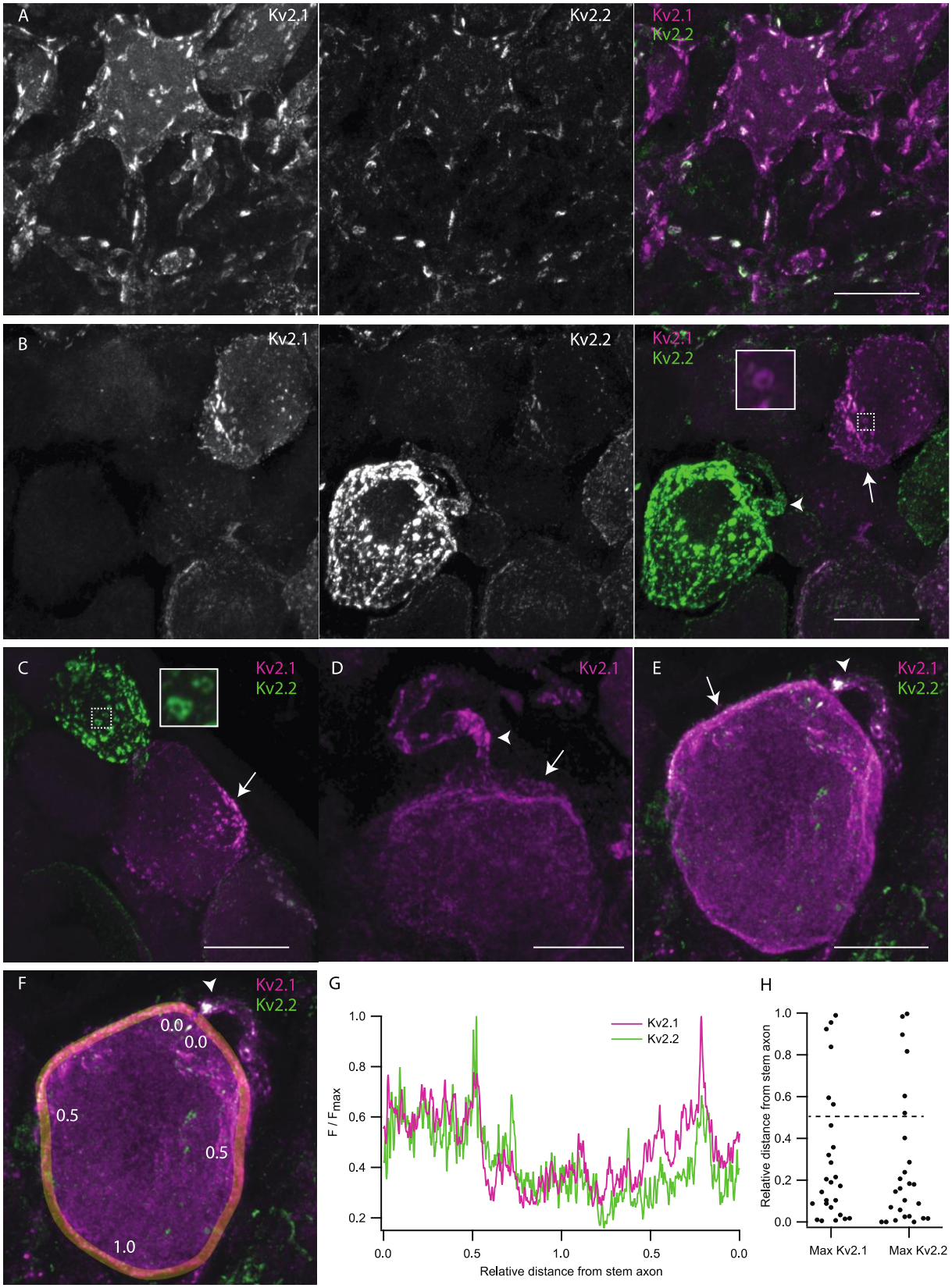
A
Kv2.1
Kv2.2
Kv2.1
Kv2.2
B
Kv2.1
Kv2.2
Kv2.1
Kv2.2
C
Kv2.1
Kv2.2
D
Kv2.1
E
Kv2.1
Kv2.2
F
Kv2.1
Kv2.2
0.0
0.0
0.5
0.5
1.0
G
Kv2.1
Kv2.2
F / Fmax
1.0
0.8
0.6
0.4
0.2
0.0
0.5
1.0
0.5
0.0
Relative distance from stem axon
H
Relative distance from stem axon
1.0
0.8
0.6
0.4
0.2
0.0
Max Kv2.1
Max Kv2.2

919 **Figure 7 legend**

920 Kv2 channels form clusters on DRG neuron somas and stem axons that are distinct from Kv2
921 channel clusters on ventral horn neurons. ***A***, Z-projection of anti-Kv2.1 and anti-Kv2.2
922 immunofluorescence in a ventral horn neuron from the 1st lumbar vertebra of a 7 week old
923 male mouse. ***B***, Z-projection of anti-Kv2.1 and anti-Kv2.2 immunofluorescence in DRG neurons
924 from the same mouse and section of the spinal column as neuron shown in A. Inset is
925 enlargement of the Kv2.1 donut cluster in dotted box. ***C***, Z-projection of anti-Kv2.1 and anti-
926 Kv2.2 immunofluorescence in DRG neurons from the same mouse as A and B. Inset is
927 enlargement of the Kv2.2 donut cluster in dotted box. ***D***, Z-projection of anti-Kv2.1
928 immunofluorescence in DRG neuron from the 13th thoracic DRG of a 24 week old male mouse.
929 ***E***, Z-projection of anti-Kv2.1 and anti-Kv2.2 immunofluorescence in DRG neuron from same
930 mouse in D. ***F***, Exemplar ROI for analyzing localization of Kv2 channel density relative to stem
931 axon. Same image as E. ROI line width is 1.24 µm. Numbers along line indicate approximate
932 distance from stem axon normalized to the midpoint of the line. ***G***, Anti-Kv2.1 (magenta) and
933 anti-Kv2.2 (green) immunofluorescence intensity along the ROI shown in F. Distance along the
934 line was normalized such that the stem axon is 0 and the midpoint of the line is 1. ***H***, Analysis of
935 the relative distance from the stem axon of the max anti-Kv2.1 or anti-Kv2.2
936 immunofluorescence. Dotted line represents the middle of neurons relative to the stem axon.
937 In all images arrows indicate asymmetrical clusters of Kv2 channels while arrowhead indicate
938 the apparent stem axons. Display settings are not identical between images. Scale bars are 20
939 µm.

940

941 **Figure 8**

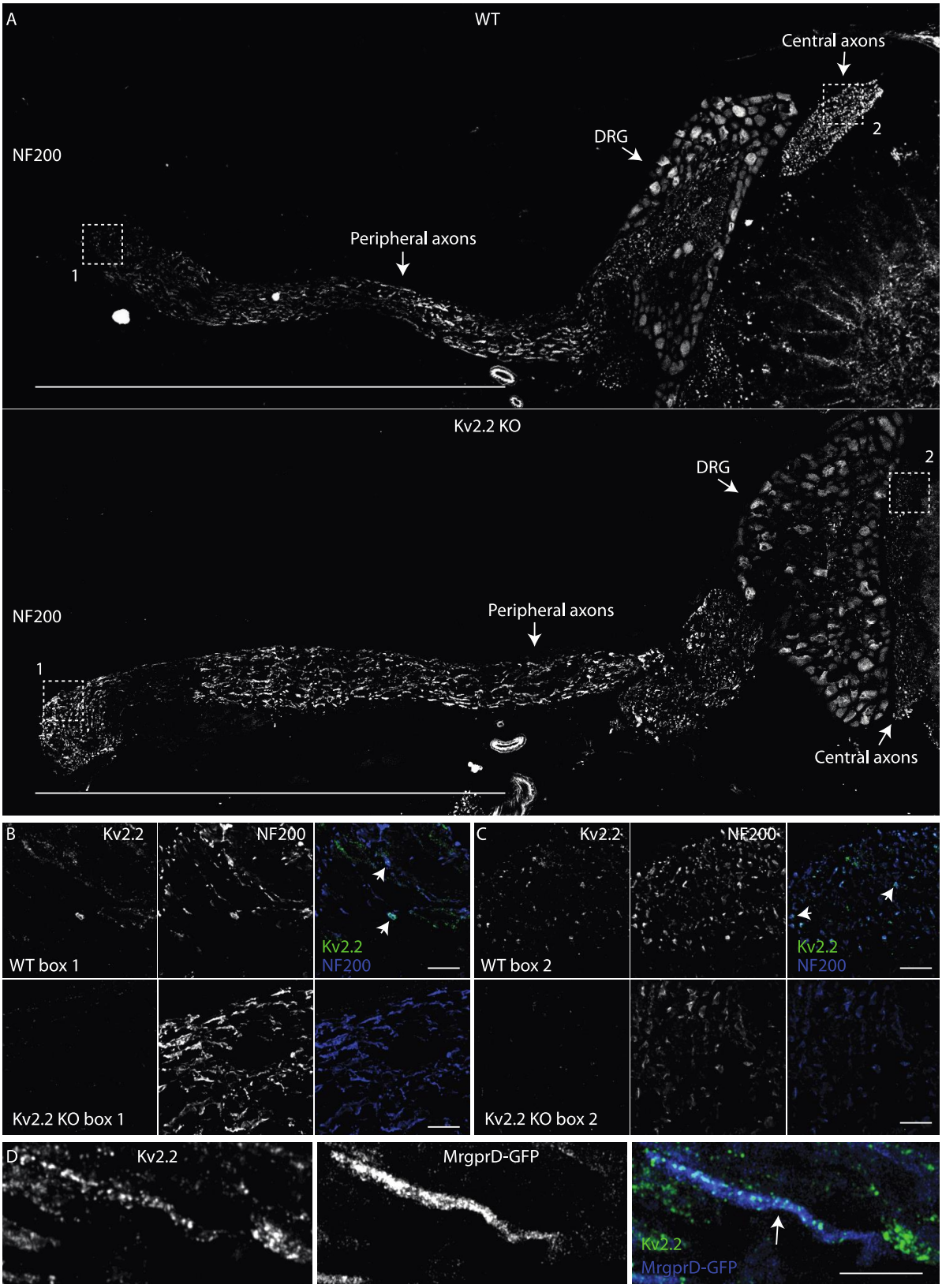

942

943 **Figure 8 legend**

944 Kv2.2 channels are expressed in peripheral axons of DRG neurons at the paranodes and
945 juxtaparanodes. ***A***, WT (top) and Kv2.2 KO (bottom) sections containing the DRG, peripheral
946 and central axons from the 1st lumbar DRG in age and sex matched 7 week old mice
947 immunolabeled for NF200 (white). Scale bar is 1 mm. ***B***, High magnification z-projection of anti-
948 Kv2.2 and anti-NF200 immunofluorescence from box 1 in A of WT and Kv2.2 KO mice. Arrows
949 indicate myelinated axons which show prominent anti-Kv2.2 immunofluorescence. Scale bars
950 are 20 µm. ***C***, High magnification z-projection of anti-Kv2.2 and anti-NF200
951 immunofluorescence from box 2 in A of WT and Kv2.2 KO mice. Arrows indicate myelinated
952 axons which show prominent anti-Kv2.2 immunofluorescence. Scale bars are 20 µm. ***D***, High
953 magnification z-projection of anti-Kv2.2 immunofluorescence and MrgprD-GFP fluorescence in
954 the peripheral axons of the 12th thoracic DRG of a 13 week old MrgprD-GFP mouse. Arrow
955 indicates anti-Kv2.2 immunofluorescence on a GFP^{+} axon. Scale bar is 10 µm.

956 **Figure 9**

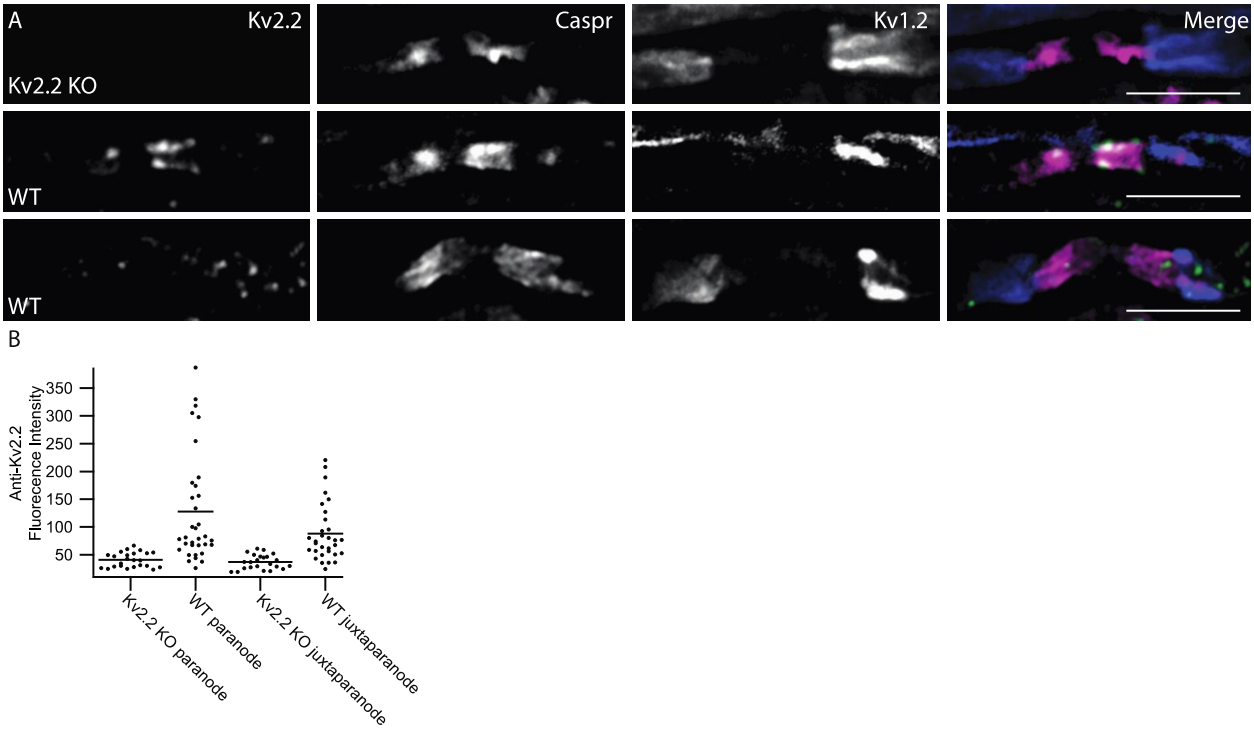

957

958 **Figure 9 legend**

959 Kv2.2 is expressed at the paranodes and juxtaparanodes of DRG neuron axons. ***A***, Kv2.2 KO

960 (top) and WT (middle and bottom) sections containing the peripheral axons from the 12th

961 thoracic DRG in 28 week old mice immunolabeled for Kv2.2, Caspr and Kv1.2. Middle panels are

962 an exemplar of prominent Kv2.2 immunofluorescence in the paranodes of DRG neurons and

963 bottom panels are an exemplar of prominent Kv2.2 clusters in the juxtaparanodes. Scale bars

964 are 5 µm. ***B***, Analysis of anti-Kv2.2 immunofluorescence intensity in the paranodes and

965 juxtaparanodes of age and sex matched WT and Kv2.2 KO mice. Individual points represent a

966 single paranode or juxtaparanode identified by anti-Caspr or anti-Kv1.2 immunofluorescence.

967 **Figure 10**

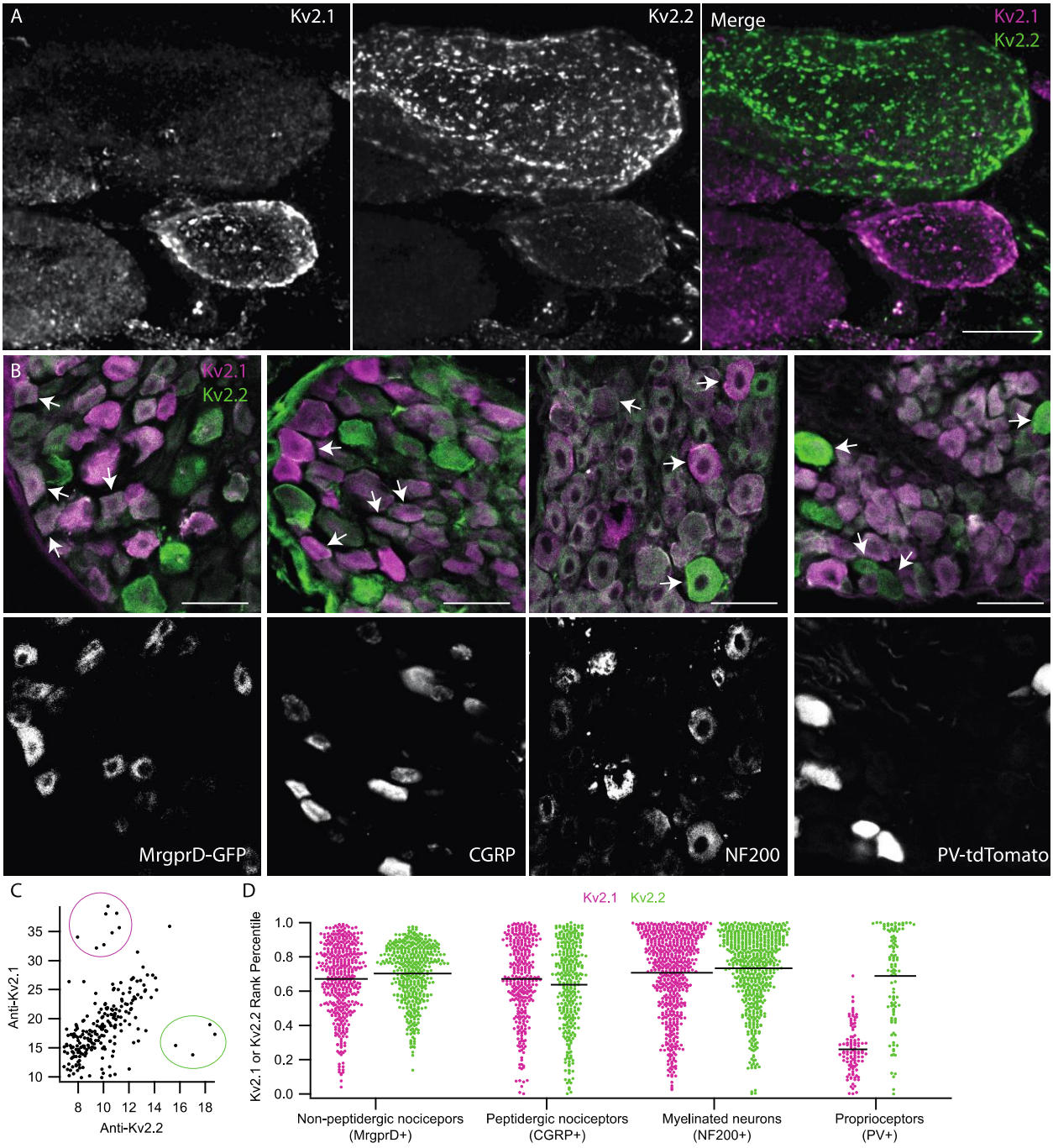

968

969 **Figure 10 legend**

970 Anti-Kv2 immunofluorescence intensities are non-uniform across DRG neuron subtypes. ***A***,

971 Exemplar z-projection of enrichment of anti-Kv2.1 (magenta) or anti-Kv2.2 (green)

immunofluorescence in neighboring neurons. DRG section is from a 10 week old male mouse. Scale bar is 10 µm. ***B***, Top images show anti-Kv2.1 (magenta) and anti-Kv2.2 (green) immunofluorescence in DRG sections where subpopulation specific markers were used to identify, from left to right, non-peptidergic nociceptors, peptidergic nociceptors, myelinated neurons and proprioceptors. Fluorescence from specific markers is shown in bottom panels. Arrows indicate four exemplar neurons that have clear positivity for each subpopulation identified by fluorescence in lower panels. CGRP and NF200 subpopulations were identified using anti-CGRP and anti-NF200 antibodies while MrgprD-GFP and PV-tdTomato subpopulations were from transgenic mouse lines. Scale bars are 50 µm. ***C***, Scatter plot of anti-Kv2.1 and anti-Kv2.2 immunofluorescence of individual neurons. Each point represents one neuron. Magenta circle highlights the subpopulation of neurons that have high anti-Kv2.1 but low anti-Kv2.2 immunofluorescence while the green circle highlights the subpopulation of neurons that have high anti-Kv2.2 but low anti-Kv2.1 immunofluorescence. ***D***, Ranked anti-Kv2.1 immunofluorescence (magenta points) or ranked anti-Kv2.2 immunofluorescence (green points) of individual neurons from subpopulations shown in B. Only neurons that were positive for each marker are shown. Each point represents one neuron. MrgprD population N = 4 mice, CGRP population N = 3 mice, NF200 population N = 3 mice and PV population N = 2 mice.

990 **Figure 11**

991

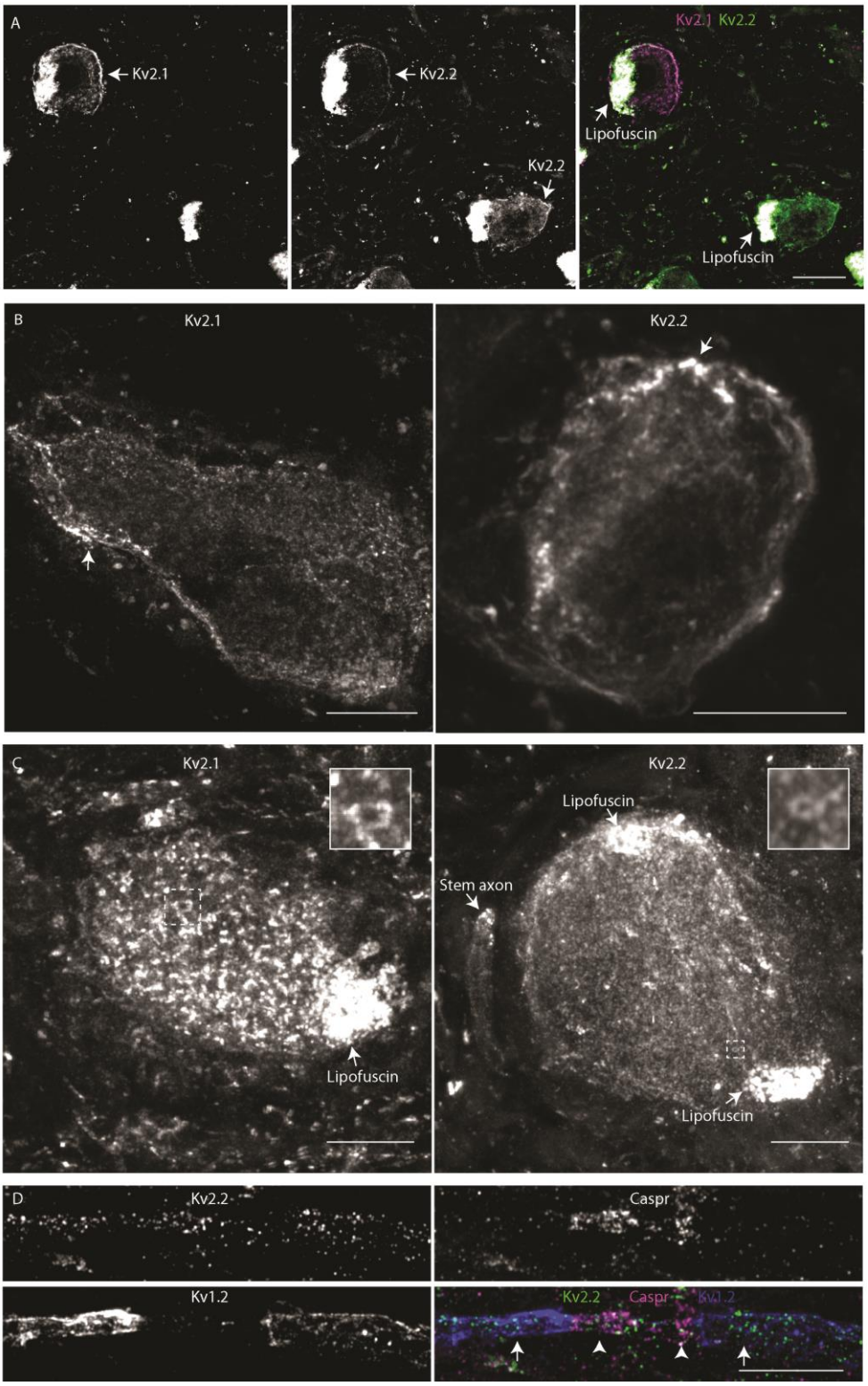

992

993 **Figure 11 legend**

994 Kv2 channel expression and localization in human DRG neurons is similar to mice. ***A***,
995 Immunofluorescence from human DRG neurons labeled with anti-Kv2.1 and anti-Kv2.2
996 antibodies. Autofluorescence attributed to lipofuscin is labeled in right panel while apparent
997 Kv2.1 and Kv2.2 protein are labeled in left and middle panel respectively. Scale bar is 50 µm. ***B***,
998 Z-projection of anti-Kv2.1 (left) and anti-Kv2.2 immunofluorescence (right) of human DRG
999 neuron somata. Arrows indicate asymmetric distribution of Kv2.1 and Kv2.2 clusters on neuron
1000 somata. Apparent lipofuscin autofluorescence was not present in these neurons. Scale bars are
1001 20 µm. ***C***, Z-projection of anti-Kv2.1 (left) and anti-Kv2.2 immunofluorescence (right) of human
1002 DRG neuron somata. Insets show expansion of dotted line boxes which highlight donut shaped
1003 Kv2.1 and Kv2.2 clusters. Arrow in right image shows anti-Kv2.2 immunofluorescence on the
1004 apparent stem axon of DRG neuron. Scale bar is 20 µm. ***D***, Z-projection of anti-Kv2.2 (upper
1005 left), anti-Caspr (upper right) and anti-Kv1.2 (bottom left) immunofluorescence of human DRG
1006 axon. Arrows in merge image (lower right) indicate juxtaparanodes and arrowheads indicate
1007 paranodes. Scale bar is 10 µm.

1008 Table 1

Figure	Genotype	Number of Mice (N)	Sections/plates Analyzed	Neurons Analyzed (n)	Age (Weeks)	Sex	Level of spinal column	Total Neurons analyzed
1	WT	1	1	124	11	M	L	115
2	WT	5	3,4,10,8,4	52,172,476,437,134,	13,7,7,7,7	M,M,F,M,M	L,T12,T12,T12,T12	1271
	Kv2.1 KO	5	4,7,5,4,5	232,124,236,293,239,	13,7,7,7,7	M,M,F,M,M	L,T12,T12,T12,T12	1124
3	WT	8	4,11,4,6,4,4,4,6	238,673,126,1227,706,748,602,572,	50,50,50,7,7,24,7,28	M,M,M,M,M,M,M,F	L,T12,T12,T12,T12,T12,L1,T12	4892
	Kv2.2 KO	8	3,6,7,4,4,4,4,5	359,400,209,853,913,719,729,745,	50,50,50,7,7,24,7,28	M,M,M,M,M,M,M,F	L,T12,T12,T12,T12,T12,L1,T12	4927
4	WT	10	7,5,6,9,8	444,268,167,669,600,	50,50,50,50,50	F,F,F,M,M	T12,T12,T12,T12,T12	3419
	Kv2.1 KO	7	5,6	298,324,	50,50	M,M	T12,T12	622
	WT	8	same as data in figure 3					
	Kv2.2 KO	8	same as data in figure 3					
5	WT	3	4,16,17,	104,379,328,	18,19,19	F,F,F	L,L,L	811
	Kv2.1 Kv2.2 DKO	2	5,14,	108,274,	18,19	F,F	L,L	382
6	WT DRG	5	1,1,1,1,1	139,51,30,40,38	10,10,10,8,8	M,M,F,F,M	T12,T8,L1,L1,L1	298
	WT Ventral Horn	5	1,1,1,1,1	75,51,23,24,28	10,10,10,8,8	M,M,F,F,M	T12,T8,L1,L1,L1	201
7	WT	2	2	N/A	7,24	M,M	L1,T12	N/A
8	WT	1	1	N/A	7	M	L1	N/A
	Kv2.2 KO	1	1	N/A	7	M	L1	N/A
	MrgprD-GFP	1	1	N/A	13	F	T12	N/A
9	WT	1	1	N/A	28	F	T12	N/A
	Kv2.2 KO	1	1	N/A	28	F	T12	N/A
10	WT	1	1	N/A	10	M	L5	N/A
	MrgprD-GFP	4	6,5,9,14	852,632,842,1392,	13,20,8,8	F,M,F,F	T12,L1,L1,L1	3718
	WT	5	7,4,6,7,4	482,464,592,641,166,	7,10,24,19,19	F,M,M,F,F	L1,T12,T12,T12,T12	2345
	PV-tdTomato	2	15,9	1978,1158,	8,8	F,M	L1,L1	3136
1-1	WT	1	1	N/A	10	M	L5	N/A
1-2	WT	1	1	N/A	28	M	L	N/A

1-3	WT	1	3	125	13	M	L	125
2-1	WT	1	33	5399	8	M	T11 and T12	5399
2-2	MrgprDGFP	1	1	N/A	13	F	T12	N/A
2-3	MrgprDGFP	4	6,15,9,14	5,568,769,051,487	14,20,8,8	F,M,F,F	L1,L1,L1,L1	3824
	WT	2	7,5	771,478	24,8	M,F	L1,L1	1249
6-1	WT DRG	4	1,1,1,1	25,30,28,35	7,7,8	M,F,F,F	L1,L1,L1,L1	118
	WT Ventral Horn	4	1,1,1,1	17,19,26,19	7,7,8	M,F,F,F	L1,L1,L1,L1	81
7-1	MrgprDGFP	1	1	N/A	14	F	T12	N/A
	WT	2	1,1	N/A	11,17	M,M	L,L	N/A
8-1	WT	1	1	N/A	7	F	T12	N/A
	Kv2.1 KO	1	1	N/A	7	F	T12	N/A

Table 1 legend

Detailed information on mice used in each figure. In columns “Sections/Plates Analyzed”, “Neurons Analyzed”, “Age”, “Sex” and “Level of Spinal Column” information for each mouse is separated by commas. In column “Level of Spinal Column” L1 refers to the first lumbar DRG and T12 refers to the twelfth thoracic DRG and if only L is shown the specific DRG is not known but the DRG is from the lumbar region.

1017 Table 2

Antigen	Antibody name	Species/isotype	Manufaturer information	Concentration used	RRID	Figures
Kv2.1	K89/34	Mouse IgG1 mAb	NeuroMab	6.7 ug/mL	AB_10672253	1, 2, 3, 4,6-1, 7, 8-1, 10, 11, 11-1, 11-2
Kv2.2	Kv2.2c	Rabbit pAb	In-house Trimmer laboratory	1:100 purified from strip assay	AB_2801484	3, 4, 6-1, 7, 8, 9, 10, 11, 11-1, 11-2,11-3
Nav1.8	N134/12	Mouse IgG2a mAb	NeuroMab	1:5 tissue culture supernatant	AB_10672261	1,11-1
Kv2.1	K89/34R	Mouse IgG2a mAb	In-house Trimmer laboratory	1:5 tissue culture supernatant	AB_2315768	11-1
beta III Tubulin	NA	Rabbit pAb	Abcam ab18207	0.33 ug/mL	AB_444319	2, 8-1
Kv2.2	N372B/60	Mouse IgG2b mAb	NeuroMab	1 ug/mL	AB_2315868	1, 1-3, 6, 10
NF200	NA	chicken pAb	Abcam ab4680	0.2 ug/mL	AB_304560	3, 8, 10
Caspr	K65/35	Mouse IgG1 mAb	NeuroMab	1:5 tissue culture supernatant	AB_2877274	9
Kv1.2	K14/16	Mouse IgG2b mAb	NeuroMab	1:5 tissue culture supernatant	AB_2877295	9,11
CGRP	NA	Rabbit pAb	Immunostar	1:1000	AB_572217	10
DsRed	NA	Rabbit pAb	Takara Cat#632543	0.17 ug/mL	AB_2307319	10
Nav1.7	N68/6	Mouse IgG1 mAb	NeuroMab	1:5 tissue culture supernatant	AB_2184355	11-1,11-3

1018

1019

1020 **Table 2 legend**

1021 Detailed information on antibodies used throughout the manuscript. In column “Concentration

1022 Used” if only dilution is given concentration was unknown however, tissue culture supernatant

1023 concentrations of antibodies typically range between 15-30 µg/mL. **SUPPLEMENTAL FIGURES**

1024 **Figure 1-1**

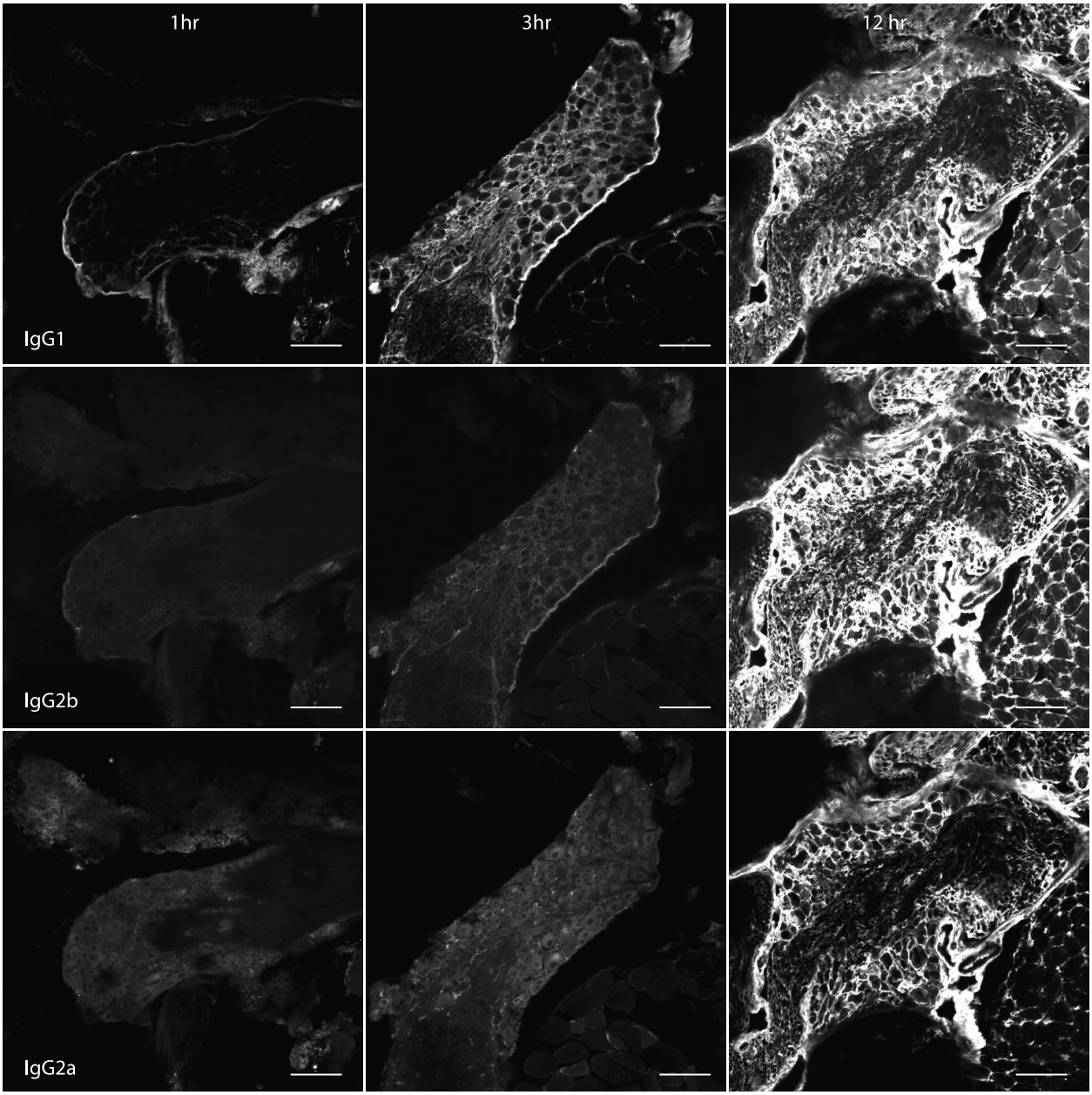

1025

1026 **Figure 1-1 legend**

1027 Off target mouse anti-IgG1, IgG2b and IgG2a immunofluorescence increases with fixation time.

1028 Images of DRG sections labeled with fluorescently tagged antibodies which target IgG1 (top),

1029 IgG2b (middle) and IgG2a (bottom) after DRG were fixed in ice cold 4% PFA for 1, 3 and 12

1030 hours. DRG sections are from the same mouse. Scale bars are 100 µm.

1031

1032 **Figure 1-2**

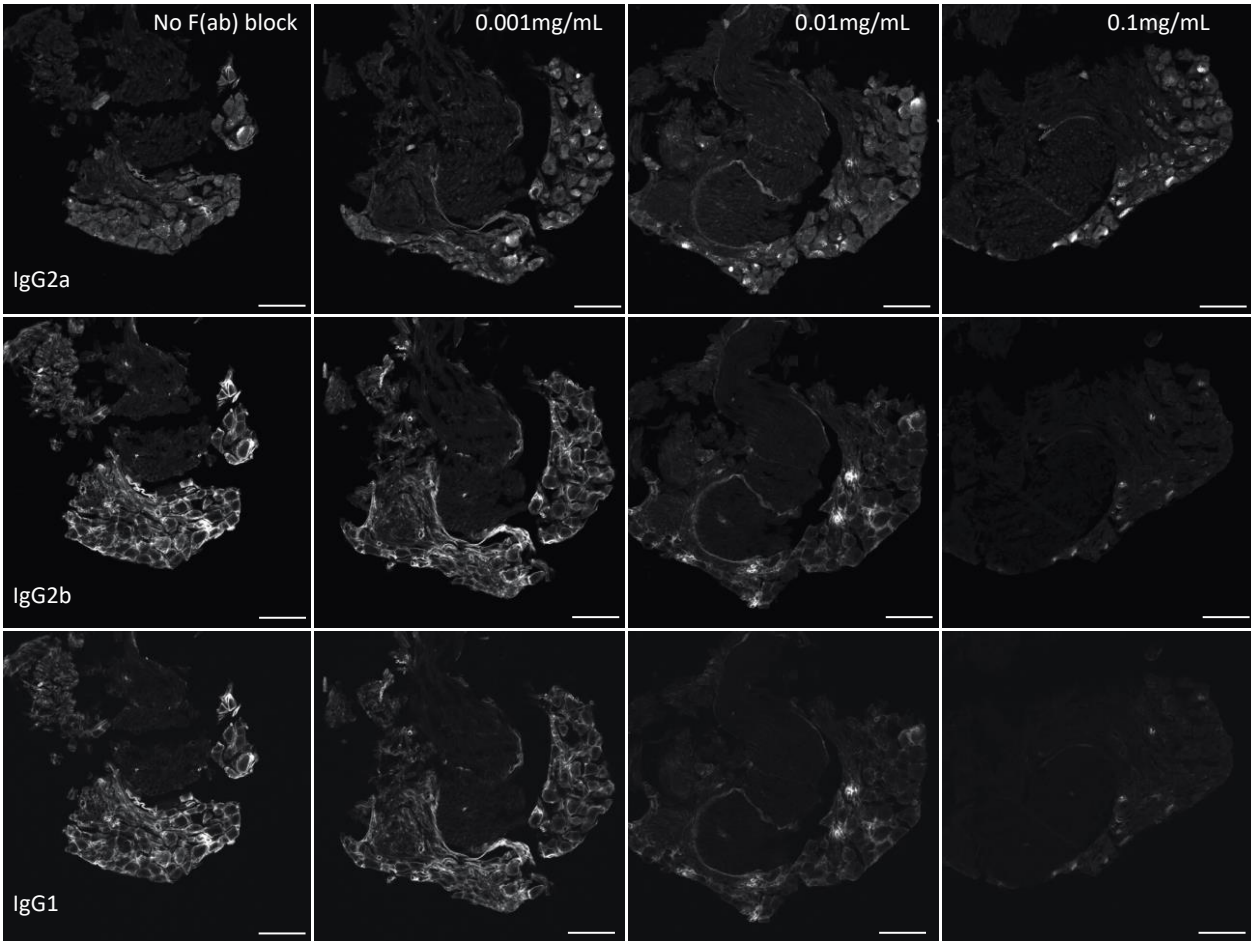

1033

1034 **Figure 1-2 legend**

1035 Pre-incubation of mouse DRG sections in IgG H+L Fab fragments reduces off target secondary
1036 antibody labeling. Representative images of DRG sections from the same DRG treated with
1037 increasing concentrations (left to right) of IgG H+L Fab fragment and the same concentration of
1038 secondary antibody used in experiments throughout this study. Images were taken with
1039 identical imaging settings and are set to the same brightness and contrast. Scale bars are 100
1040 µm.

1041 **Figure 1-3**

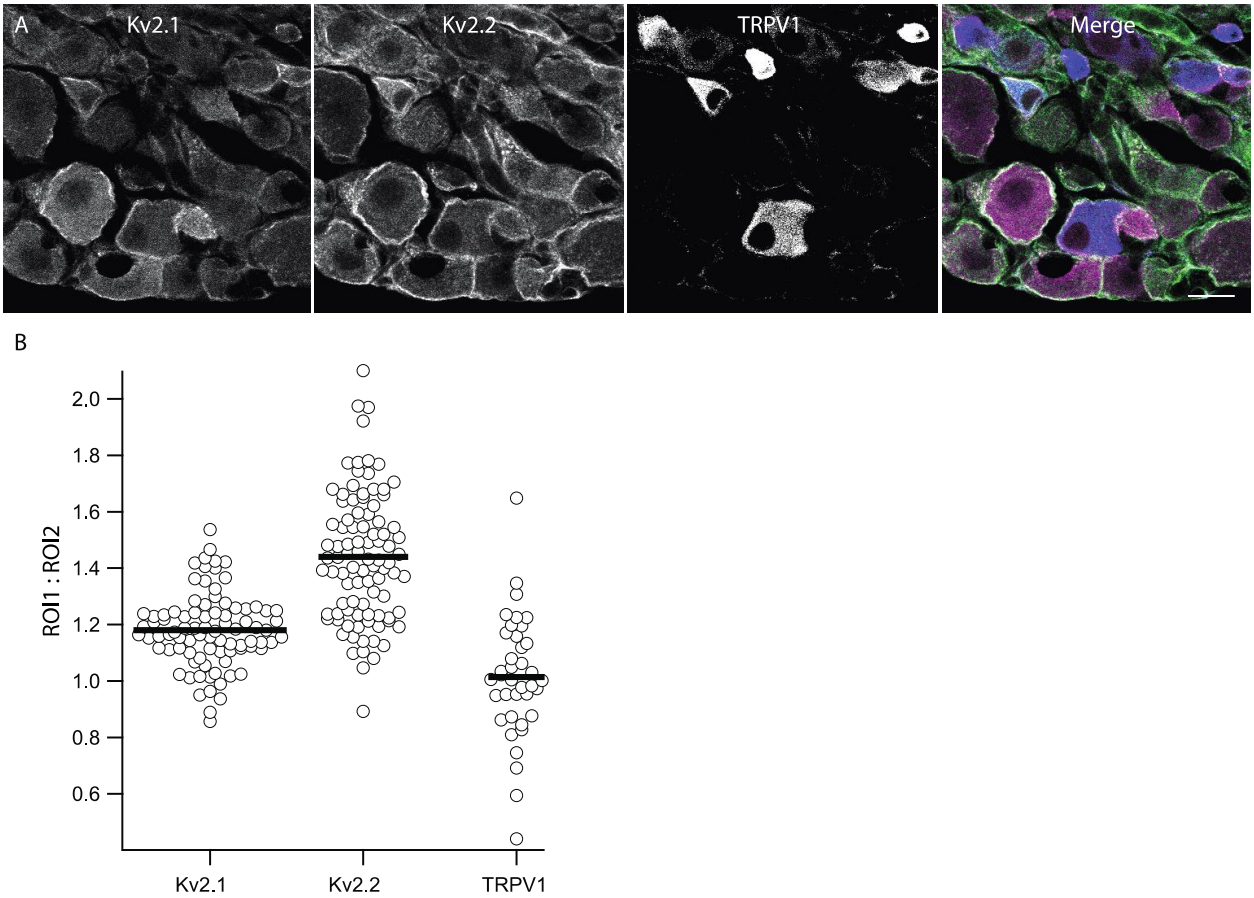

1042

1043 **Figure 1-3 legend**

1044 Kv2.1 and Kv2.2 protein are enriched at the outer edge of DRG neuron somas relative to TRPV1.

1045 ***A***, Anti-Kv2.1, anti-Kv2.2 and anti-TRPV1 immunofluorescence from lumbar DRG neurons.

1046 Prominent cytoplasmic anti-TRPV1 immunofluorescence was observed in a subset of small

1047 diameter neurons. In merge image anti-Kv2.1, anti-Kv2.2 and anti-TRPV1 immunofluorescence

1048 are magenta, green and blue respectively. Scale bar is 20 µm. ***B***, Ratio of average anti-Kv2.1,

1049 anti-Kv2.2 or anti-TRPV1 immunofluorescence from outer and inner ROIs for individual

1050 neurons.

1051

1052 **Figure 2-1**

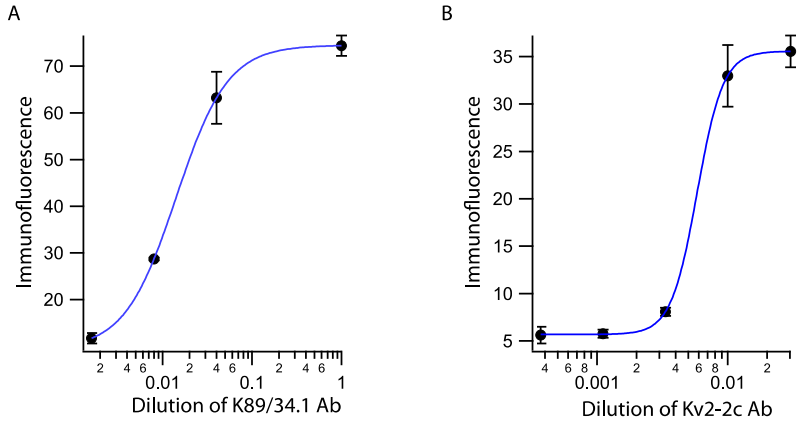

1053

1054 **Figure 2-1 legend**

1055 Kv2 antibodies used in knockout experiments are at saturating concentrations. ***A***,

1056 Concentration response of immunofluorescence from sections labeled with anti-Kv2.1 antibody

1057 used in Figure 2. Blue line is a Hill fit of the data. 1:1 = 2 sections, 1:25 = 3 sections, 1:125 = 2

1058 sections, 1:625 = 3 sections ***B***, Concentration response of immunofluorescence from sections

1059 labeled with anti-Kv2.2 antibody used in Figure 3. Blue line is a Hill fit of the data. 1:33 = 2

1060 sections, 1:100 = 10 sections, 1:300 = 4 sections, 1:900 = 4 sections, 1:2700 = 3 sections

1061

1062 **Figure 2-2**

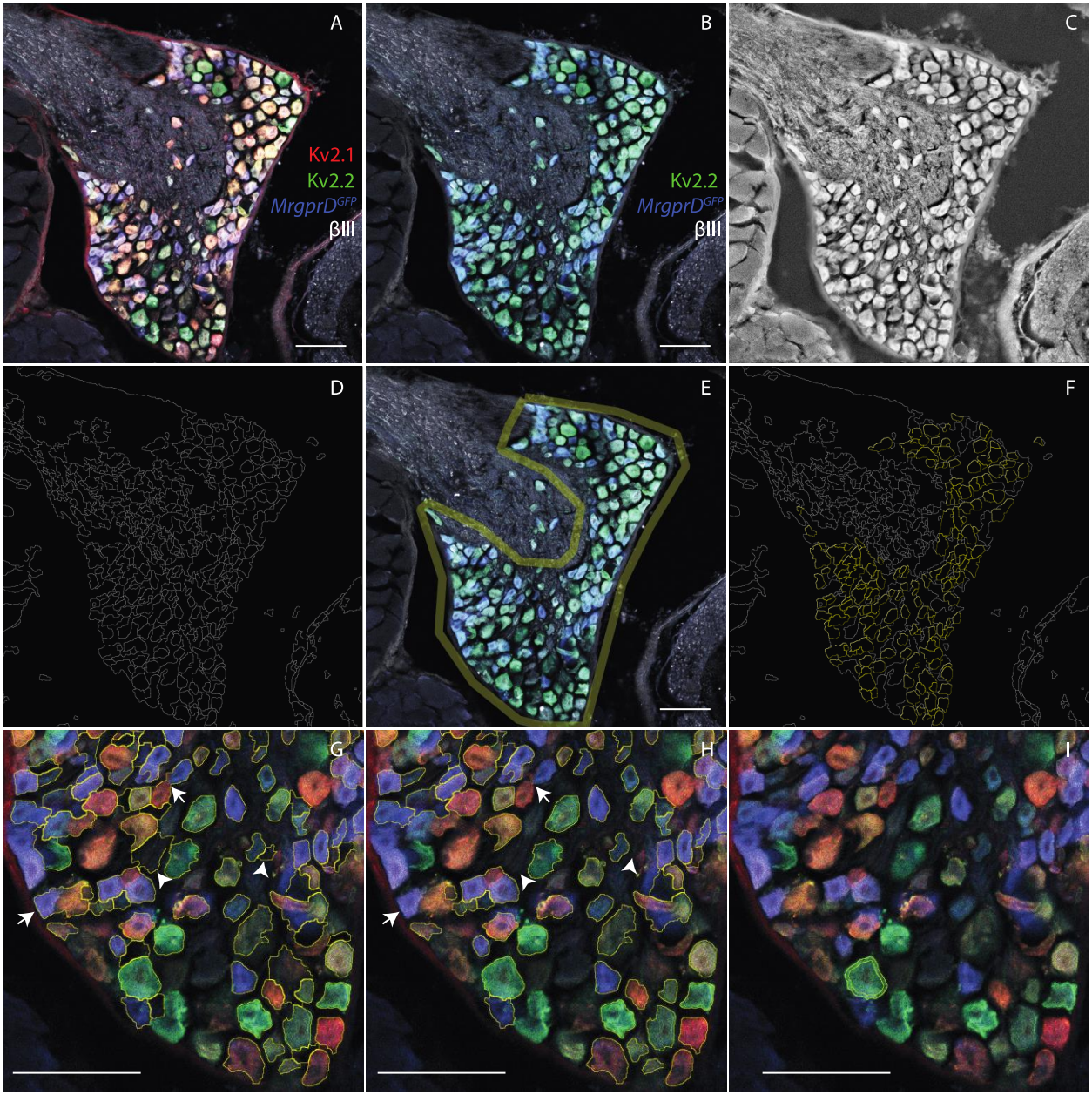

1063

1064 **Figure 2-2 legend**

1065 A method to sample neurons in DRG imaging data using watershed segmentation identifies the

1066 outer region of neurons. ***A***, Image of anti-Kv2.1, anti-Kv2.2, anti-βIII tubulin

1067 immunofluorescence and MrgprD-GFP fluorescence. ***B***, Same image as A with anti-Kv2.1

1068 immunofluorescence channel removed as this is an example of processing data for Kv2.1 KO

1069 analysis. ***C***, Grayscale image of average fluorescence from all three channels shown in B.
1070 Gaussian and median filters were applied to image to improve watershed segmentation. ***D***,
1071 Watershed segmentation of image in C using the MorphoLibJ Morphological Segmentation
1072 Plugin in Fiji. ***E***, Example of manually drawn boundary that encompasses the neuron somas in
1073 the DRG so that only these watershed lines are selected. ***F***, Selected ROIs from watershed
1074 segmentation (yellow). ROIs were excluded based on roundness and size using the Analyze
1075 Particles tool in Fiji. ***G***, ROIs in F overlaid on DRG image showing that some ROIs are selecting
1076 regions that do not contain neurons (arrow heads) or are selecting multiple neurons (arrows).
1077 ***H***, ROIs after processing using an in house R script which removes most, but not all, ROIs that
1078 do not contain neurons (arrow heads) and ROIs that contain two neurons (arrows). Each
1079 experiment performed was done alongside controls where the primary antibodies were
1080 omitted and fluorescence from these control sections was used by the in house R script to
1081 identify and remove ROIs that do not contain neurons. ***I***, Example of automatically generated
1082 annulus that encompasses the outer edge of the soma. Scale bars are 100 µm.

1083 **Figure 2-3**

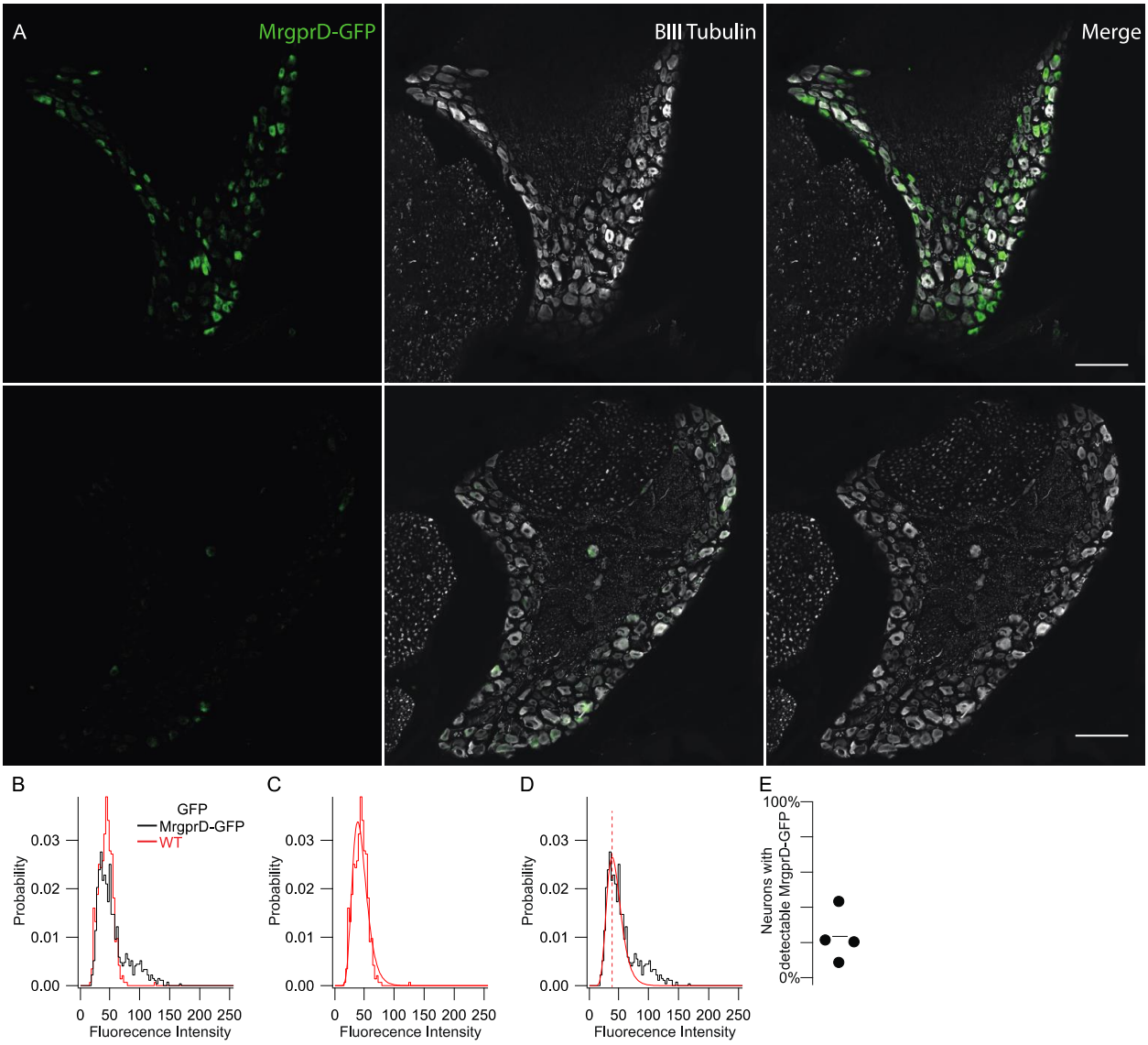

1084

1085 **Figure 2-3 legend**

1086 Method used to estimate percent of neurons expressing Kv2.1 and Kv2.2 reliably predicts the

1087 percentage of neurons that express GFP in MrgprD-GFP mice. ***A***, MrgprD-GFP (top) and WT

1088 (bottom) DRG sections immunolabeled for BIII tubulin (white). Images were taken with identical

1089 imaging settings and are set to the same brightness and contrast. Scale bars are 100 µm. ***B***,

1090 Distribution of fluorescence intensity from MrgprD-GFP (black) and WT (red) neurons. Data

1091 represents the fluorescence intensity of 905 MrgprD-GFP neurons from 9 DRG sections from 1

1092 mouse or 477 WT neurons from 5 DRG sections from 1 mouse. DRG sections were taken from 7

1093 week old female mice and are from the 1st lumbar DRG. ***C***, WT data shown in B fit with a log

1094 normal distribution (red fit). ***D***, MrgprD-GFP data shown in B fit with the WT distribution (red

1095 fit) where width and mean were constrained to the WT distribution and amplitude was

1096 unconstrained (equation 1). Only MrpgrD-GFP data to the left of the mean intensity of WT

1097 neurons (red dotted line) was used for the fit. ***E***, Percent of neurons with detectable GFP

1098 protein of 4 mice (3 females 1 male). All DRG sections were taken from the 1st lumbar DRG.

1099 **Figure 6-1**

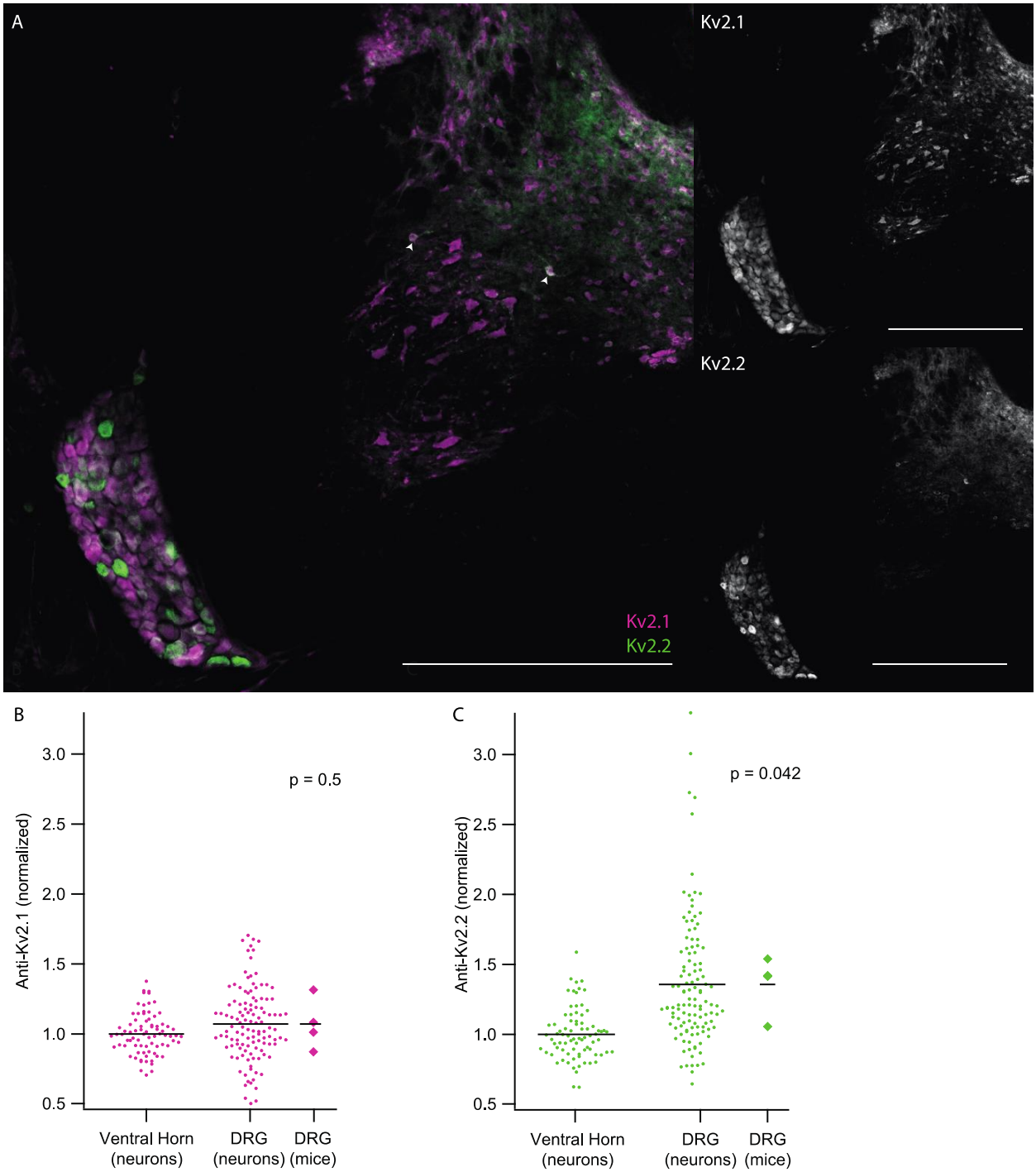

1100

1101 **Figure 6-1 legend**

1102 DRG neurons have enriched Kv2.2 protein compared to neurons in the ventral horn. ***A***, Anti-
1103 Kv2.1 (magenta) and anti-Kv2.2 (green) immunofluorescence in a spinal cord section from the
1104 13th thoracic vertebra (left). Anti-Kv2.1 immunofluorescence (right top) and anti-Kv2.2
1105 immunofluorescence (right bottom). Arrow heads show neurons in the spinal cord with anti-
1106 Kv2.2 immunofluorescence. Scale bars are 500 µm. ***B***, Anti-Kv2.1 immunofluorescence from
1107 individual neurons (circles) in the DRG and ventral horn normalized to the average fluorescence
1108 intensity of neurons in the ventral horn. Diamonds to the right of data represent the average
1109 intensity in the DRG of individual mice. Significant differences from 1 were calculated for
1110 individual mice using Students t-test. N = 4 mice n = 116 in DRG and n = 77 in ventral horn. ***C***,
1111 Identical analysis shown in B with anti-Kv2.2 immunofluorescence.

1112

1113 **Figure 7-1**

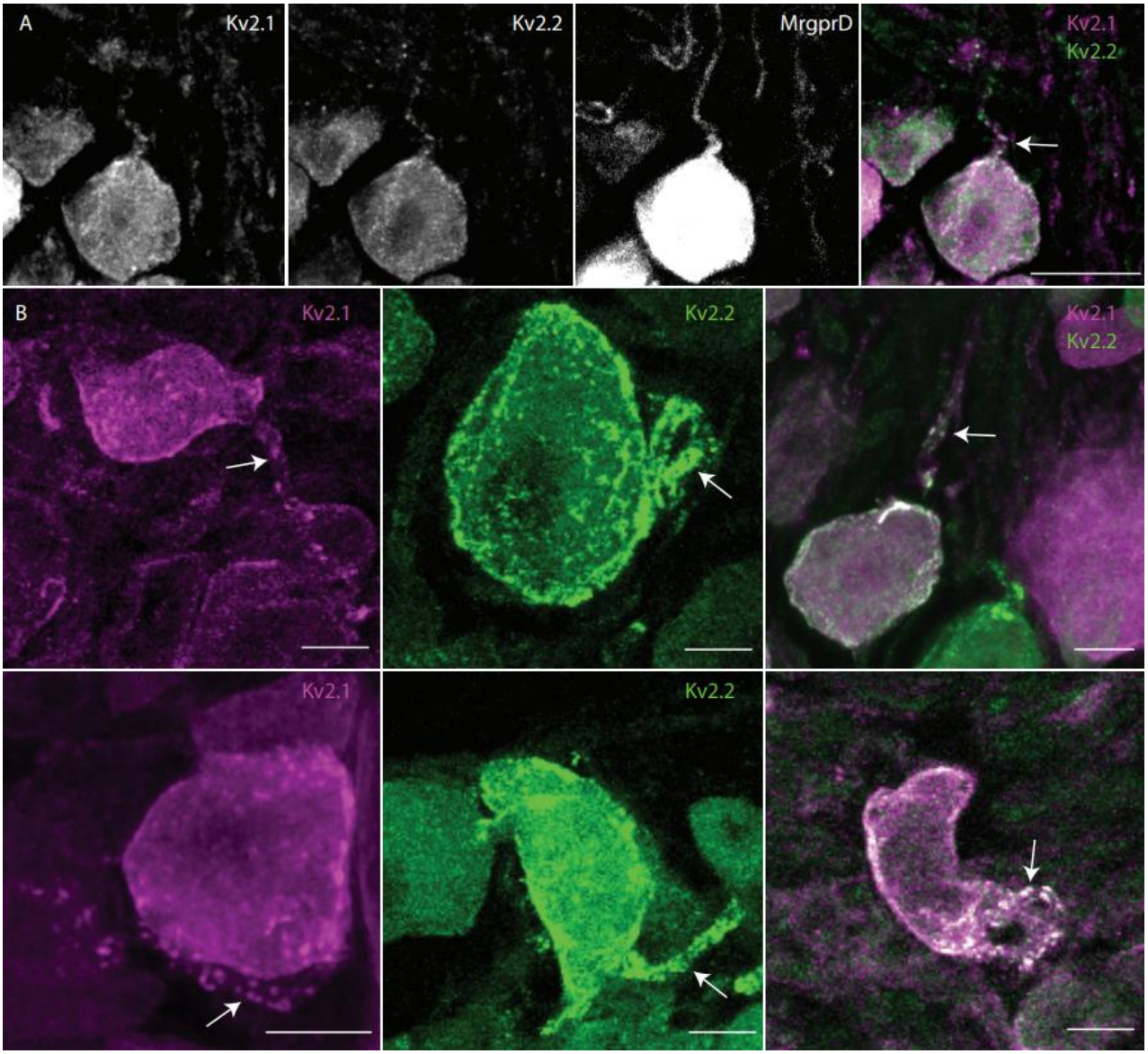

1114

1115 **Figure 7-1 legend**

1116 Kv2 channels are expressed on the stem axon of mouse DRG neurons. ***A***, Z-projection with anti-

1117 Kv2.1 and anti-Kv2.2 immunofluorescence on the stem axon of a neuron in the DRG of a

1118 MrgprD-GFP mouse. ***B***, Gallery of z-projected images of DRG neurons with anti-Kv2.1 and/or

1119 anti-Kv2.2 immunofluorescence on stem axons. Arrows indicate stem axons. Scale bars are 10

1120 µm

Figure 8-1

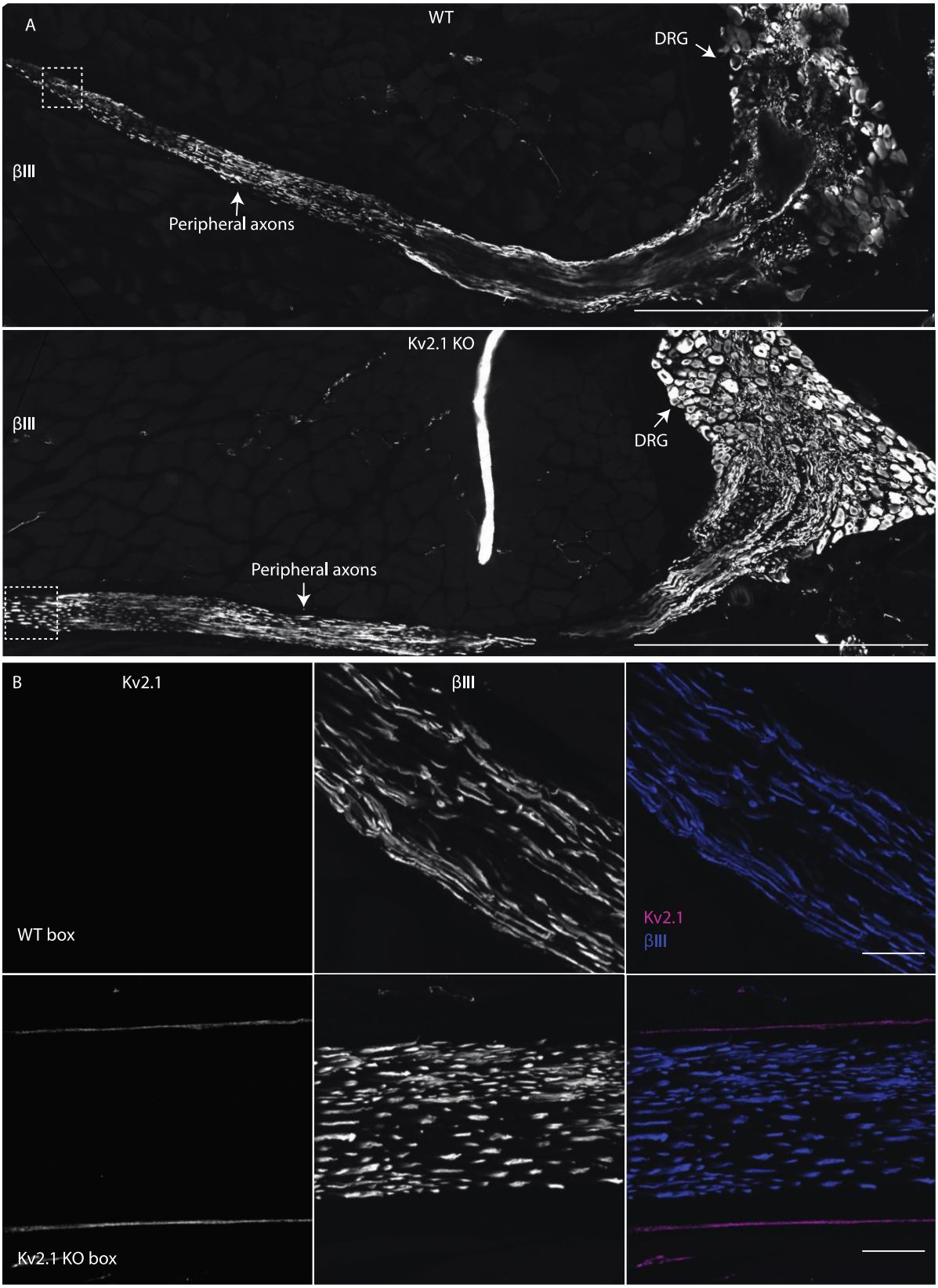
A
WT
DRG
βIII
Peripheral axons
Kv2.1 KO
βIII
DRG
Peripheral axons
B
Kv2.1
βIII
WT box
Kv2.1
βIII
Kv2.1 KO box

1123 **Figure 8-1 legend**

1124 Kv2.1 channels were not detected in peripheral axons of DRG neurons. ***A***, WT (top) and Kv2.1

1125 KO (bottom) sections containing the DRG and peripheral axons from the 12th thoracic DRG in

1126 age and sex matched 7 week old mice immunolabeled for βIII tubulin (white). Scale bar is 500

1127 µm. ***B***, High magnification z-projection of anti-Kv2.1 and anti-βIII immunofluorescence from box

1128 in A of WT and Kv2.1 KO mice. Scale bars are 20 µm.

1129

1130 **Figure 11-1**

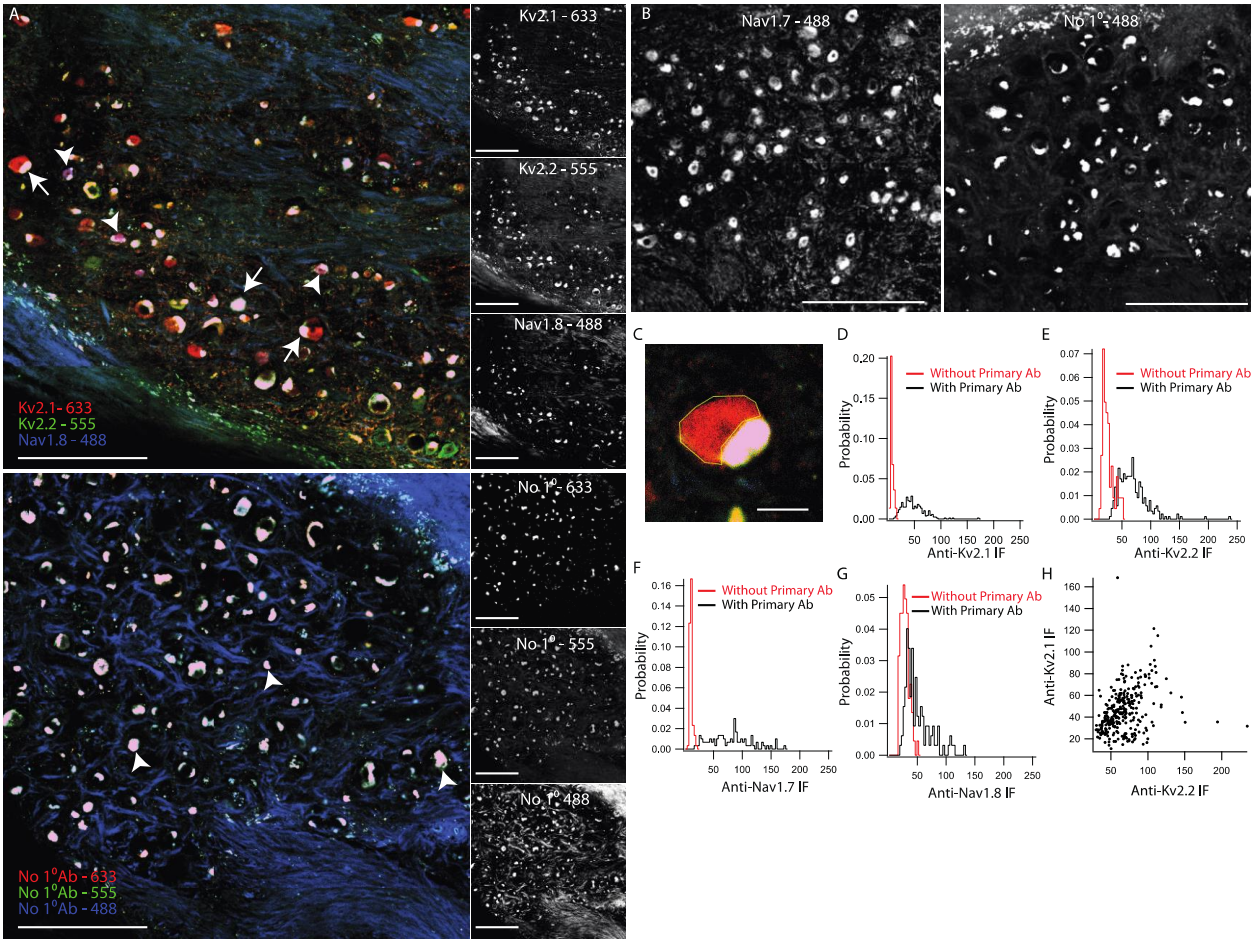

1131

1132 **Figure 11-1 legend**

1133 Fluorescence from human DRG neurons labeled with ion channel targeting antibodies is distinct

1134 from human DRG neurons where ion channel targeting antibodies were omitted. ***A***, Top:

1135 Immunofluorescence from human DRG section labeled with anti-Kv2.1, anti-Kv2.2 and anti-

1136 Nav1.8 antibodies. Bottom: Fluorescence from human DRG section where the primary

1137 antibodies are omitted. Arrows in top and bottom images indicate examples of

1138 autofluorescence from apparent intracellular lipofuscin. Arrow heads in top image identify anti-

1139 Nav1.8 immunofluorescence. Images on the right are fluorescence from each fluorescence

1140 channel of the top and bottom images. Number next to target protein label represents

1141 excitation wavelength. DRG sections from top and bottom images are from the same DRG.
1142 Scale bars are 500 µm. ***B***, Left: Immunofluorescence from human DRG section labeled with anti-
1143 Nav1.7 antibody. Right: Fluorescence from human DRG section where the primary antibody has
1144 been omitted. Number next to target protein label represents excitation wavelength. DRG
1145 sections in left and right images are from the same DRG. Scale bars are 500 µm. ***C***, Exemplar
1146 manually drawn ROI to analyze fluorescence intensity in human DRG neurons that omits
1147 apparent lipofuscin autofluorescence. Scale bar is 50 µm. ***D***, Distribution of fluorescence
1148 intensity of human DRG neurons labeled with an anti-Kv2.1 antibody (black) or when the anti-
1149 Kv2.1 antibody was omitted (red). Data represents the fluorescence intensity of 293 neurons
1150 labeled with anti-Kv2.1 antibody or 73 neurons where the anti-Kv2.1 antibody was omitted. ***E***,
1151 Distribution of fluorescence intensity of human DRG neurons labeled with anti-Kv2.2 antibody
1152 (black) or when the anti-Kv2.2 antibody was omitted (red). Data represents the fluorescence
1153 intensity of 293 neurons labeled with anti-Kv2.2 antibody or 73 neurons where the anti-Kv2.2
1154 antibody was omitted. ***F***, Distribution of fluorescence intensity of human DRG neurons labeled
1155 with anti-Nav1.7 antibody (black) or when the anti-Nav1.7 antibody was omitted (red). Data
1156 represents the fluorescence intensity of 99 neurons labeled with anti-Nav1.7 antibody or 99
1157 neurons where the anti-Nav1.7 antibody was omitted. ***G***, Distribution of fluorescence intensity
1158 of human DRG neurons labeled with anti-Nav1.8 antibody (black) or when the anti-Nav1.8
1159 antibody was omitted (red). Data represents the fluorescence intensity of 293 neurons labeled
1160 with anti-Nav1.8 antibody or 73 neurons where the anti-Nav1.8 antibody was omitted. ***H***,
1161 Fluorescence intensity of human neurons labeled with both anti-Kv2.1 and anti-Kv2.2
1162 antibodies. Individual points represent individual neurons.

1163 **Figure 11-2**

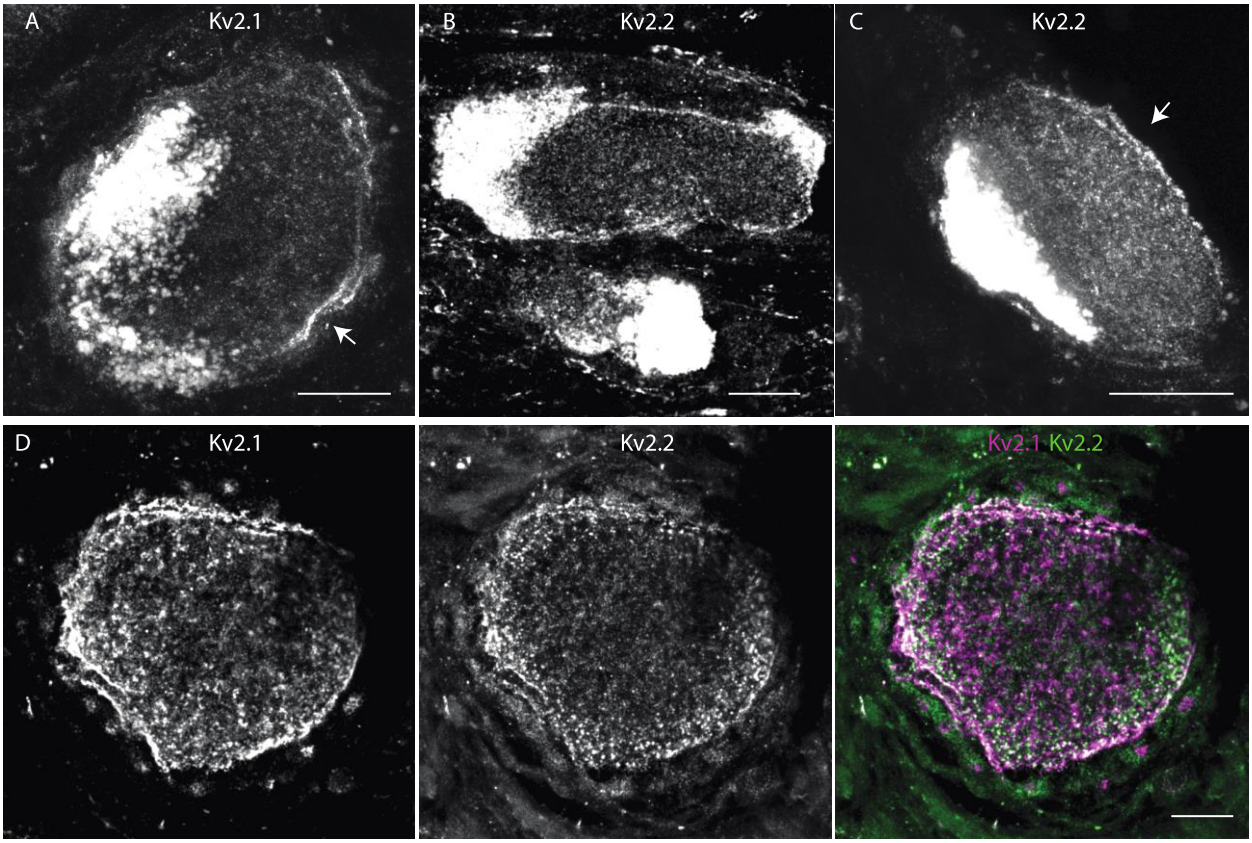

1164

1165 **Figure 11-2 legend**

1166 Kv2 channels are enriched at the outer edge of human DRG neurons. ***A***, Exemplar z-projection

1167 of anti-Kv2.1 immunofluorescence enriched at the outer surface of a human DRG neuron. Scale

1168 bar is 20 µm. ***B***, Exemplar z-projection of anti-Kv2.2 immunofluorescence enriched at the outer

1169 surface of a human DRG neuron. Scale bar is 20 µm. ***C***, Exemplar z-projection of asymmetrical

1170 anti-Kv2.2 immunofluorescence enriched at the outer surface of a human DRG neuron. Scale

1171 bar is 20 µm. ***D***, Exemplar z-projection of anti-Kv2.1 and anti-Kv2.2 immunofluorescence both

1172 enriched at the outer surface of a human DRG neuron soma. Scale bar is 20 µm.

1173

1174 **Figure 11-3**

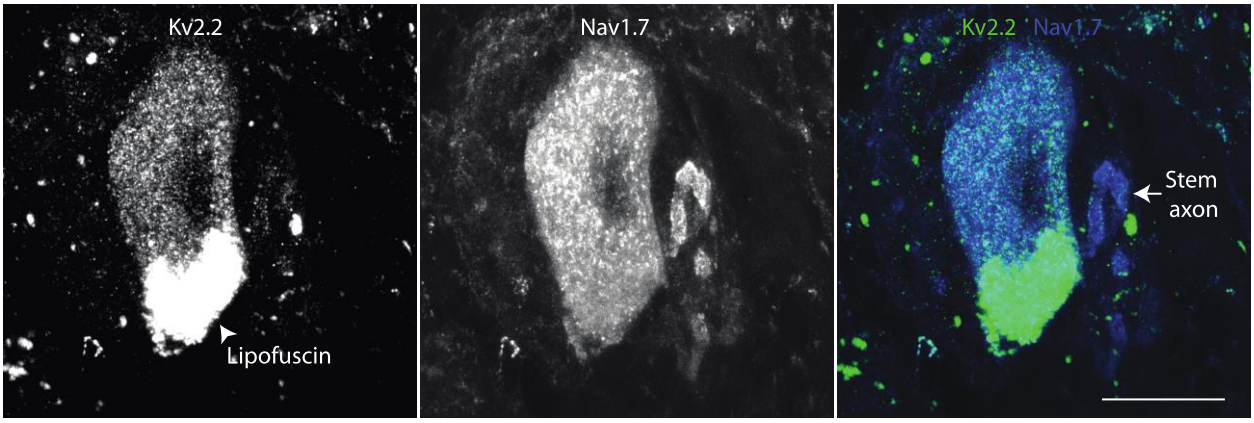

1175

1176 **Figure 11-3 legend**

1177 Z-projection of anti-Kv2.2 and anti-Nav1.7 immunofluorescence in a human DRG neuron soma

1178 and stem axon. Arrow in merge indicates the stem axon of the DRG neuron. Apparent lipofuscin

1179 autofluorescence is labeled in left panel. Scale bar is 20 µm.